Cell Reports

Article

Targeting the MITF/APAF-1 axis as salvage therapy for MAPK inhibitors in resistant melanoma

Graphical abstract

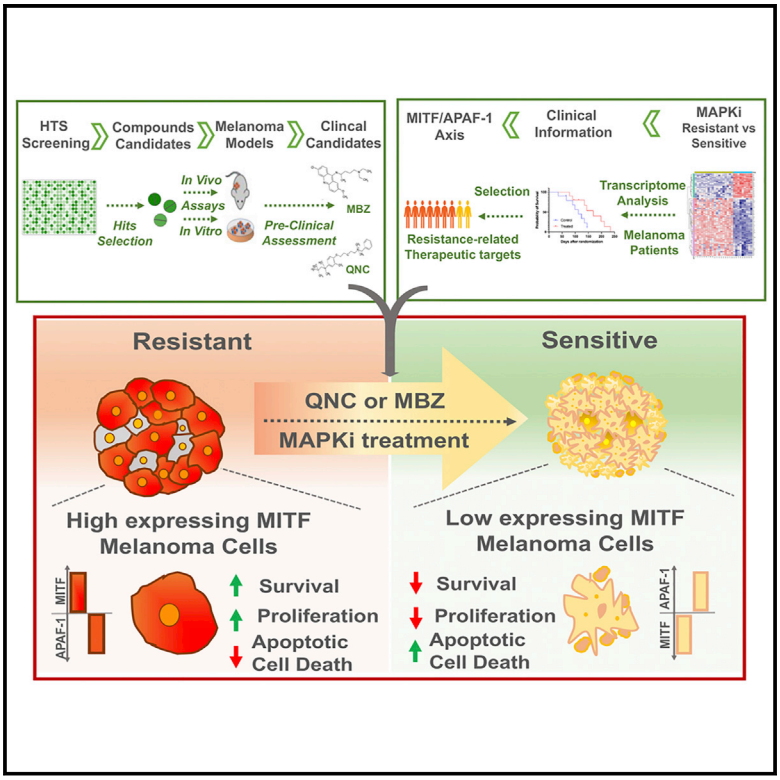

Highlights

- The MITF/APAF-1 axis is a molecular driver of MAPK inhibitor resistance
- QNC and MBZ are potent activators of apoptosome-independent cell death
- QNC and MBZ act by inhibiting specific epigenetic modulators of MITF/APAF-1
- QNC/MBZ with MAPK inhibitors: potential therapeutic approach for resistant melanoma

Authors

Pietro Carotenuto, Alessia Romano, Anna Barbato, ..., Luisa Lanfrancone, Alessia Indrieri, Brunella Franco

Correspondence

p.carotenuto@tigem.it (P.C.), franco@tigem.it (B.F.)

In brief

Carotenuto et al. show that the MITF/APAF-1 axis is a molecular driver of MAPK inhibitor resistance in melanoma. Two compounds regulating key signaling networks in melanoma, including the MITF/APAF-1 axis, were identified. The identified therapeutic approach may represent an important clinical advance in the treatment of resistant melanoma.

Carotenuto et al., 2022, Cell Reports *41*, 111601
November 8, 2022
https://doi.org/10.1016/j.celrep.2022.111601

CellPress

Cell Reports

CellPress
OPEN ACCESS

Article

Targeting the MITF/APAF-1 axis as salvage therapy for MAPK inhibitors in resistant melanoma

Pietro Carotenuto,[1,2,12,13,*] Alessia Romano,[1,12] Anna Barbato,[1] Paola Quadrano,[1] Simona Brillante,[1] Mariagrazia Volpe,[1] Luigi Ferrante,[1] Roberta Tammaro,[1] Manuela Morleo,[1,3] Rossella De Cegli,[1] Antonella Iuliano,[1,4] Marialuisa Testa,[1] Fabrizio Andreone,[1] Gennaro Ciliberto,[5] Eduardo Clery,[6] Giancarlo Troncone,[6] Giuseppe Palma,[7] Claudio Arra,[7] Antonio Barbieri,[7] Mariaelena Capone,[8] Gabriele Madonna,[8] Paolo A. Ascierto,[8] Luisa Lanfrancone,[9] Alessia Indrieri,[1,10] and Brunella Franco[1,2,11,*]

[1]TIGEM, Telethon Institute of Genetics and Medicine, 80078 Naples, Italy
[2]Department of Translational Medical Science, University of Naples "Federico II", 80131 Naples, Italy
[3]Department of Precision Medicine, University of Campania "Luigi Vanvitelli," 80138 Naples, Italy
[4]Department of Mathematics, Computer Science, and Economics (DiMIE), University of Basilicata, 85100 Potenza, Italy
[5]IRCCS, National Cancer Institute Regina Elena, 00144 Rome, Italy
[6]Department of Public Health, University of Naples "Federico II", 80131 Naples, Italy
[7]SSD Animal Unit, Istituto Nazionale Tumori-IRCCS-Fondazione "G. Pascale", 80131 Naples, Italy
[8]Melanoma, Cancer Immunotherapy and Development Therapeutics Unit, Istituto Nazionale Tumori-IRCCS-Fondazione "G. Pascale", 80131 Naples, Italy
[9]Department of Experimental Oncology, IEO, European Institute of Oncology IRCCS, 20141 Milan, Italy
[10]Institute for Genetic and Biomedical Research (IRGB), National Research Council (CNR), 20090 Milan, Italy
[11]Genomic and Experimental Medicine, Scuola Superiore Meridionale, 80138 Naples, Italy
[12]These authors contributed equally
[13]Lead contact
*Correspondence: p.carotenuto@tigem.it (P.C.), franco@tigem.it (B.F.)
https://doi.org/10.1016/j.celrep.2022.111601

SUMMARY

Melanoma is a deadly form of cancer characterized by remarkable therapy resistance. Analyzing the transcriptome of MAPK inhibitor sensitive- and resistant-melanoma, we discovered that APAF-1 is negatively regulated by MITF in resistant tumors. This study identifies the MITF/APAF-1 axis as a molecular driver of MAPK inhibitor resistance. A drug-repositioning screen identified quinacrine and methylbenzethonium as potent activators of apoptosis in a context that mimics drug resistance mediated by APAF-1 inactivation. The compounds showed anti-tumor activity in *in vitro* and *in vivo* models, linked to suppression of MITF function. Both drugs profoundly sensitize melanoma cells to MAPK inhibitors, regulating key signaling networks in melanoma, including the MITF/APAF-1 axis. Significant activity of the two compounds in inhibiting specific epigenetic modulators of MITF/APAF-1 expression, such as histone deacetylases, was observed. In summary, we demonstrate that targeting the MITF/APAF-1 axis may overcome resistance and could be exploited as a potential therapeutic approach to treat resistant melanoma.

INTRODUCTION

Melanoma is the deadliest form of skin cancer, accounting for ~80% of skin cancer-related deaths (Fischer et al., 2018). It is characterized by high aggressiveness and remarkable therapy resistance due to mechanisms supporting cell survival (Rajkumar and Watson, 2016). Over 85% of melanomas harbor mutations in BRAF, NRAS, and NF1 genes. These events activate the MAP kinase (MAPK) pathway, which in turn promotes cell proliferation, melanoma initiation, and progression (Paluncic et al., 2016). Currently, patients with BRAF mutated metastatic melanoma are eligible for therapy with MAPK inhibitors (MAPKi). Unfortunately, although the anti-tumor responses to MAPKi have shown some success, resistance to therapy remains a clinical challenge (Rajkumar and Watson, 2016). Despite the fact that immunotherapeutic approaches have benefited ~50% of patients, a large proportion of melanomas are unresponsive or resistant to treatment (Luke et al., 2017). Thus, new strategies to target resistant melanomas and improve patient survival are required. The mechanisms of resistance established during melanoma progression often depend on the ability of cancer cells to evade apoptosis. The inactivation of the pro-apoptotic gene APAF-1 has been observed in several tumors, including melanoma (Jia et al., 2001; Liu et al., 2002; Soengas et al., 2001; Wolf et al., 2001; Yamamoto et al., 2000). It has been suggested that loss of APAF-1 and its transcriptional silencing may impair the apoptotic pathway, thus promoting resistance to therapy. Indeed, experimental evidence indicates that APAF-1-negative melanomas are drug resistant and unable to execute the typical apoptotic program (Soengas et al., 2001;

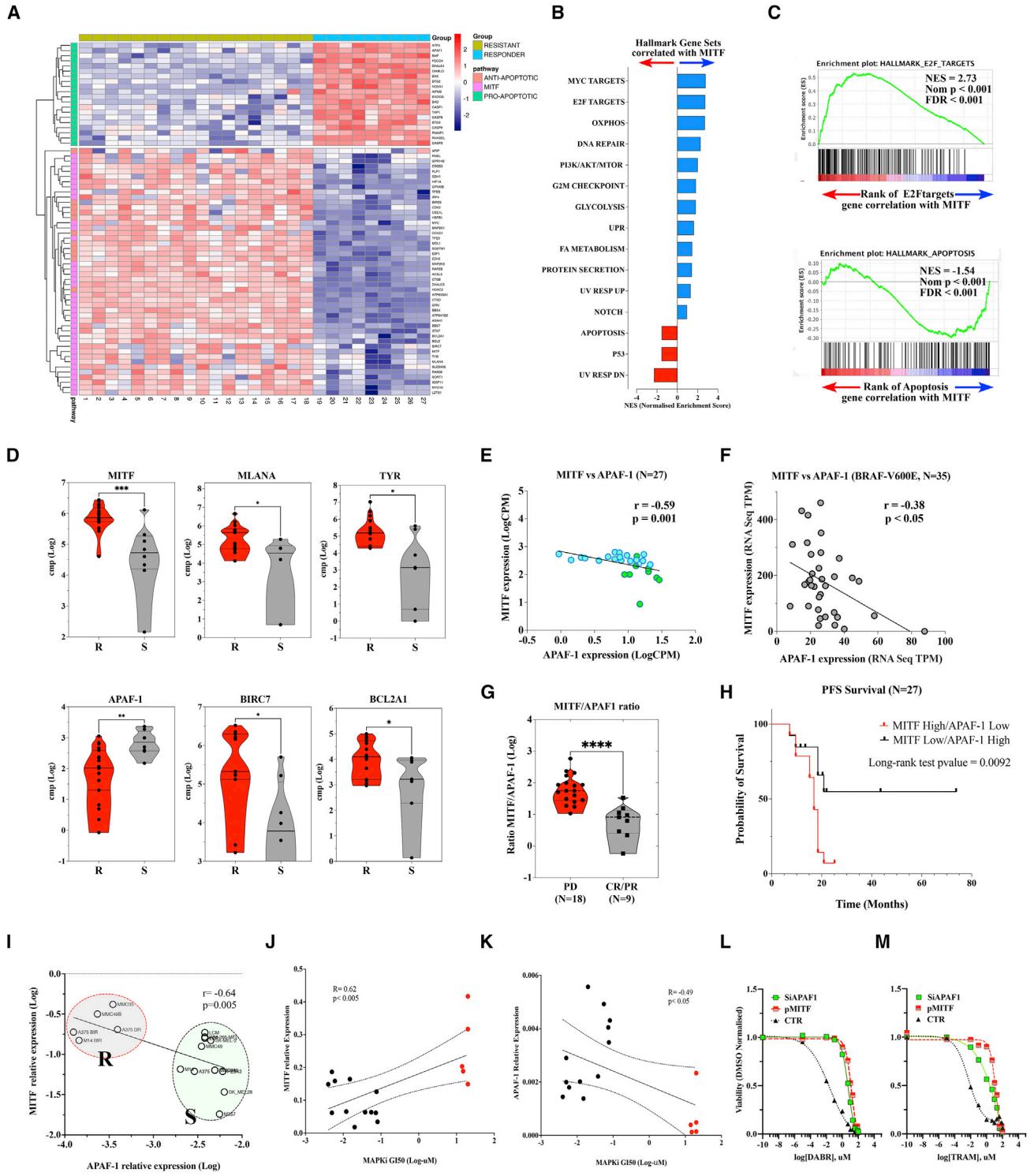

Figure 1. MITF and APAF-1 expression correlates with MAPKi resistance in melanoma

(A) Patients were grouped in RESPONDER (n = 9) or RESISTANT (n = 18) to MAPKi. Hierarchical clustering using RNA-seq data unbiasedly separated responder and resistant patients. Gene expression profiles of the MITF and apoptotic transcriptional programs between patients are shown. Color annotations indicate the transcriptional program and patient subgroups.

(B and C) GSEA with compiled modules from Hallmarks in MSigDB. Bar graphs represent the gene sets, showing normalized enrichment score (NES) > 2.0 and false discovery rate (FDR) q < 5%.

(legend continued on next page)

Dai et al., 2004; Zanon et al., 2004). We discovered that the survival melanoma oncogene MITF mediates APAF-1 inactivation, thus we hypothesize that the MITF/APAF-1 axis may represent a mechanism to escape from apoptosis. As such, we sought to identify compounds that target the MITF/APAF-1 axis, sensitize tumors to standard therapy, or trigger apoptosis in resistant melanoma. The identification of drugs that can overcome functional inactivation of the apoptotic program represents an important clinical advance in the treatment of resistant melanoma.

RESULTS

APAF-1 expression is associated with response to MAPKi and is dependent on the MITF program

We performed whole-transcriptome sequencing (RNA-seq) on tumor tissues obtained from 27 patients diagnosed with advanced metastatic melanomas. These patients displayed mutations in BRAF (V600E) and underwent treatment with MAPKi (Table S1). By using best RECIST criteria response, patients were divided in "responder" (n = 9) and "resistant" (n = 16). Differential expression (DE) analysis between the two groups indicated the MITF and apoptotic transcriptional programs as the most de-regulated gene networks (Figure 1A).

We analyzed and compared the expression levels of MITF and its target genes (Tirosh et al., 2016) and found that the MITF-related gene network was highly enriched in the resistant group (Figure 1A). MITF expression increases in response to MAPKi and can contribute to MAPK pathway inhibitor resistance (Pathria et al., 2016; Smith et al., 2016; Wellbrock and Arozarena, 2015). We confirmed that upregulation of the MITF program correlated with the expression of multiple survival, pro- and anti-apoptotic genes (Figure 1A). Gene set enrichment analysis (GSEA) identified several gene networks significantly modulated by MITF expression (Figure 1B), including those involved in oncogenic (MYC/E2F targets) and metabolic processes (glycolysis, OXPHOS, FA metabolism) (Figures 1B and 1C). Moreover, high MITF expression was associated with negative enrichment of the apoptotic gene network (Figures 1B and 1C). Accordingly, MITF upregulation in melanoma patients correlated with increased expression of its targets MLANA and TYR and of the anti-apoptotic genes BCL2A1 and BIRC7 in the resistant group (Figures 1D and S1A), also indicating that MITF plays a functional role (Frederick et al., 2013).

We analyzed and compared the levels of APAF-1 between responder and resistant and observed a reduction in gene expression levels in the resistant group (Figure 1D). A negative correlation between MITF and APAF-1 expression was found in our patient cohort (Figure 1E) and confirmed in an independent cohort (SKCM-DFCI) of metastatic melanoma (van Allen et al., 2015) (Figure S1B) and in the BRAF mutated dataset (Figure 1F). In our cohort, MAPKi-resistant melanomas reported increased MITF expression correlated with concomitant down-regulation of APAF-1 (Figures 1E and S1C–S1E), thus highlighting that reduced expression of APAF-1 correlated with MAPKi resistance. This inverse correlation led us to hypothesize that MITF may modulate APAF-1 inactivation in resistant melanoma.

To further dissect the impact of MITF/APAF-1 reciprocity on patient response, we stratified the patients into MITF high/APAF-1 low and MITF low/APAF-1 high. In our cohort, the MITF high/APAF-1 low transcriptional state was associated with poor response to MAPKi treatment (Figures 1G and S1F). Moreover, progression-free survival-based (PFS) analysis of the two groups demonstrated that MIFT low/APAF-1 high patients showed significantly improved PFS (Figure 1H). Conversely, PFS was significantly shorter in the MIFT high/APAF-1 low group (median 16.9 versus 73 months; Figure 1H). Moreover, patients with the MIFT low/APAF-1 high status had significantly better OS than those with MIFT high/APAF-1 low (Figures S1G and S1H).

To investigate the contribution of the MITF/APAF-1 axis in establishing MAPKi resistance, we used a panel of commercial and patient-derived cell lines (Tables S3 and S4). We also benefited from the use of BRAFi- (A375-BIR, M14-BIR) and MAPKi-resistant (A375-DR) cells (Table S3). Analysis of MITF and APAF-1 expression revealed that MAPKi-resistant melanoma cells showed significantly increased levels of MITF with reduced expression of APAF-1 (Figures 1I and S1I). Moreover, we observed that the GI_{50} of MAPKi correlated with MITF and APAF-1 expression levels (Figures 1J and 1K), suggesting that the MITF/APAF-1 axis may contribute to MAPKi treatment response.

(C) Representative GSEA plots of E2F targets and apoptosis gene signatures. NES, Nom p value and FDR are reported. Genes ranked based on correlation with MITF expression.

(D) Violin plots showing expression of MITF, MLANA, TYR, APAF-1, BIRC7, and BCL2A1 (CPM log) in 27 patients grouped in resistant (R) and responder (S) to MAPKi; the upper/lower quartile and the median were indicated.

(E and F) Inverse relationship between MITF and APAF-1 expression levels in BRAF-mutant melanoma tumor specimens of our cohort (E) and the SKCM-DFCI cohort (F). Linear regression indicated within dot plot (green and blue dots indicate responder and resistant samples, respectively); RNA-seq data are plotted in logCPM and logTPM scale.

(G) Comparison of MITF/APAF-1 expression ratio (log) between sensitive (CR, PR) and resistant (PD) melanoma according to RECIST criteria. Data show violin plots indicating the upper/lower quartile and the median.

(H) Kaplan-Meier estimates PFS of patients with different MITF/APAF-1 expression ratio. Patients were stratified by medians into MITF high/APAF-1 low and MITF low/APAF-1 high groups. Pairwise log-rank test was used to analyze survival; p = 0.0092.

(I) Comparison of MITF and APAF-1 expression between MAPKi-sensitive (S) and -resistant (R) melanoma cells according to their GI_{50} (Table S6). Linear regression indicated within dot plot. RT-PCR expression data are plotted in log-log scale.

(J and K) Pearson correlation analysis for MITF (J) and APAF-1 (K) expression and the GI_{50} values for MAPKi (DABR+TRAM) in the melanoma cell panel. Data are plotted in log-log scale. Red and black dots indicate MAPKi-resistant and -sensitive cells, respectively.

(L and M) Dose-response curves (mean ± SEM) for DABR and TRAM using A375 cells transfected with either CTR- or APAF-1-specific siRNAs (siAPAF1) or an expression vector for MITF (pMITF) Statistical analyses conducted by unpaired t test or one-way ANOVA with Tukey's post hoc analysis. *p < 0.01, **p < 0.001, ***p < 0.0001.

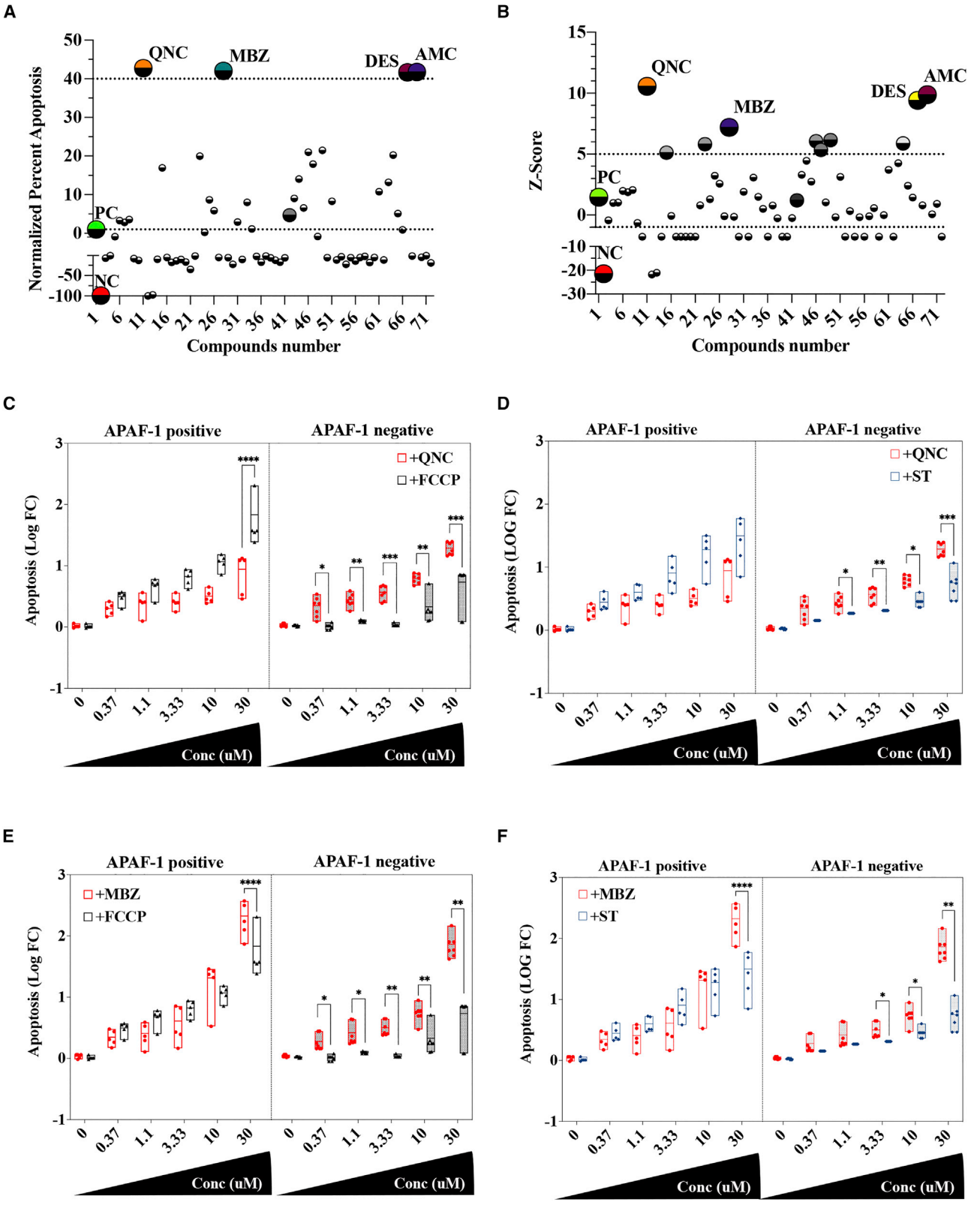

(legend on next page)

We designed *in vitro* experiments to study the functional role of the MITF/APAF-1 axis in regulating MAPKi resistance. APAF-1 depletion from A375 cells via RNAi impacted resistance to DABR and TRAM treatments, significantly increasing the GI_{50} compared with control-treated cells (Figures 1L, 1M, and S1J). Similar results were obtained by MITF overexpression (Figures 1L and 1M), thus confirming previous reports showing that MITF may drive resistance to MAPKi (Smith et al., 2016). Long-term treatment of A375 cells in which MITF was overexpressed or APAF-1 silenced impacted on MAPKi efficacy in inhibiting colony growth (Figure S1K). Interestingly, overexpression of MITF induced downregulation of APAF-1 in melanoma cells, as revealed by RT-PCR (Figure S1J) and by immunoblot analysis on A375 cells (Figure S1L). MITF silencing in BRAFi-resistant melanoma cells (A375-BIR and M14-BIR) significantly increased APAF-1 expression (Figure S1M), thus demonstrating a functional link between MITF and APAF-1 in resistant cells.

Epigenetic silencing of APAF-1 has been described in melanoma (Dai et al., 2004; Soengas et al., 2001; Zlobec et al., 2007). The DNA methyltransferase DNMT1 and histone methyltransferase EZH2 were reported to participate in epigenetic silencing of tumor-suppressor genes, including APAF-1, in different human cancers (Hinz et al., 2007; Furukawa et al., 2005) and in epigenetic reprograming inducing resistance to BRAFi in melanoma (Khaliq and Fallahi-Sichani, 2019). We further investigated their role in epigenetic silencing of APAF-1 modulated by the MITF/APAF-1 axis. In melanoma cells resistant to MAPKi, DNMT1, and EZH2 mRNAs were significantly upregulated (Figure S1I) and the expression of both genes was significantly induced by MITF overexpression (Figures S1L and S1N). However, MITF silencing induced significant downregulation of their expression (Figure S1M). Furthermore, RNAi depletion of DNMT1 and EZH2 significantly restored APAF-1 expression (Figures S1O and S1P), suggesting that both genes play a role in regulating MITF-mediated silencing of APAF-1.

These data demonstrate that MITF-mediated APAF-1 repression contributes to MAPKi resistance, proposing MITF/APAF-1 as an actionable target in metastatic melanoma.

High-throughput drug screening identified QNC and MBZ as pro-apoptotic agents

To identify novel apoptosis-inducing compounds in cells resistant to apoptotic stimuli, we screened a small molecule library using an APAF-1-deficient MEF cell line (APAF-1-KO) (Figures 2A, 2B, and S2D) (Cecconi et al., 1998). Due to the absence of APAF-1, these cells cannot initiate apoptosome-dependent mitochondrial apoptosis. Immuno-blot analysis demonstrated that targeted deletion of APAF-1 disrupted apoptosome-mediated caspase (CASP) activation in APAF-1 KO treated with staurosporine (ST) (Figure S2A).

A high-content/high-throughput drug screening (HTS) identified compounds activating apoptosome-independent cell death (Figures 2A, 2B, and S2D), which we previously showed may be activated by FCCP (carbonyl cyanide p-trifluoromethoxyphenylhydrazone) (Indrieri et al., 2013). Thus, we selected FCCP as positive control. APAF-1-KO cell sensitivity to FCCP treatment was demonstrated by immunoblot assay using CASP-9 activation as apoptotic marker (Figure S2B) and by an independent caspase-activity assay (Figure S2C).

The primary screen resulted in 70 positive hits that were re-analyzed in a double validation screening. Four compounds were selected: QNC (quinacrine); MBZ (methylbenzethonium chloride); AMC (aminacrine); and DES (desloratadine) (Figures 2A, 2B, S2D, S2E, and S2F–S2M; Table S2). Analysis of dose-response relationships identified QNC and MBZ as the most prominent compounds showing dose-dependent effects on stimulating apoptosome-independent caspase-mediated cell death (Figure S2N).

Previous work reported that APAF-1-negative melanomas are resistant to cytotoxic agents and unable to execute the apoptotic program (Soengas et al., 2001; Zanon et al., 2004; van Allen et al., 2015). To confirm that the HTS strategy led to functionally active hits in cancer, we tested QNC and MBZ for their ability to induce apoptosis in a panel of melanoma cells grouped as APAF-1-positive and -negative based on APAF-1 expression (Figures S3A and S3B). We examined the apoptosis-inducing potential of QNC and MBZ, demonstrating that both drugs efficiently induced caspase-mediated cell death in a concentration-dependent manner in all tested cell lines (Figures S3E and S3F). A parallel analysis showed that QNC and MBZ induced apoptosis more efficiently than FCCP (Figures 2C and 2E) and ST (Figures 2D and 2F) in APAF-1-negative cells. Significant differences in the level of apoptosis were found between APAF-1-positive and -negative cells in response to QNC and MBZ (Figures S3C and S3D), suggesting that APAF-1-negative cells are more sensitive to QNC- and MBZ-induced apoptosis.

Our data show that QNC and MBZ can efficiently induce apoptosis in APAF-1-negative melanoma cells, suggesting potential therapeutic use in apoptosome defective resistant melanomas.

QNC and MBZ suppress tumor growth in melanoma cells by inducing apoptosis

The anti-tumor effect of QNC and MBZ was assessed using a cell proliferation assay on melanoma cells selected for BRAF/NRAS mutational status and APAF-1 expression (Table S3; Figures S3A and S3B). Both drugs markedly suppressed cell viability in a dose-dependent manner and cells exhibited heterogeneous response profiles (Figures 3A and 3B; Table S3).

As therapeutic efficacy also depends on long-term effects, we evaluated the impact of QNC and MBZ in a colony-forming assay

Figure 2. Drug screening identified apoptosome-independent cell death-inducing compounds

(A and B) Four active compounds identified in primary HTS against MEF APAF-1 KO with respect to normalized percent of apoptosis (A) and *Z* score (B) calculated from negative controls (NC) (red) with inactive compounds (gray), active compounds (colored), positive control (PC) (light green).

(C–F) Effect of QNC (C and D) and MBZ (E and F) on apoptosis against APAF-1-positive and -negative cells in comparison with FCCP (C–E) and ST (D–F). Results are expressed as fold change (log) with respect to untreated controls (three independent experiments). Horizontal lines within the bar plots represent the 75th and 25th percentiles and the median, respectively. Statistical analyses were conducted by unpaired t test or one-way ANOVA or two-sided Wilcoxon's rank-sum test. *$p < 0.05$, **$p < 0.001$, ***$p < 0.0001$, ****$p < 0.00001$.

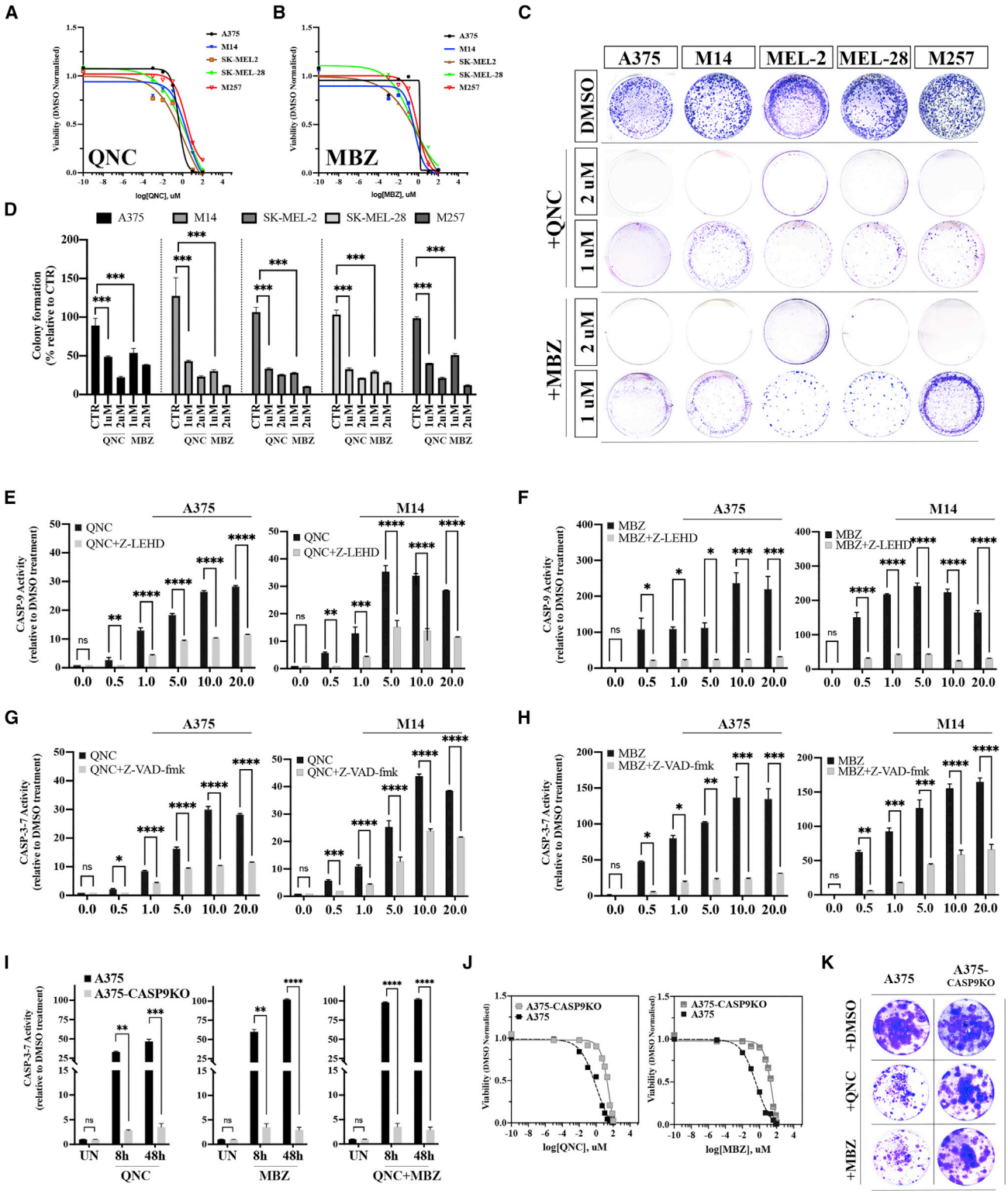

Figure 3. QNC and MBZ suppress melanoma growth *in vitro*, activating apoptosis

(A and B) Dose-response curves of A375, M14, SK-MEL-2, SK-MEL-28, and M257 cells according to sensitivity to QNC (A) and MBZ (B) (Table S3).

(C and D) Colony-formation assays of melanoma cells treated with different concentrations of QNC and MBZ (C). Representative images shown. (D) Quantification of visible colonies. The colony number in the DMSO group was set as 100%.

(legend continued on next page)

Results demonstrated that both treatments significantly reduced the number of colonies (Figures 3C and 3D), indicating that both drugs have a marked inhibitory effect on cell proliferation (Figures 3C and 3D).

To confirm that QNC and MBZ suppressed tumor growth by inducing cell death, we performed analysis of apoptosis. The analysis of CASP-9 activation after treatment with increasing concentrations of QNC and MBZ demonstrated that both drugs can induce CASP-9 activation in a dose-dependent manner (Figures S3G and S3H). Immuno-blotting analysis revealed increased levels of cleaved CASP-9 and PARP in QNC- and MBZ-treated A375 and M14 cells (Figure S3I), confirming both drugs can induce apoptosis to suppress cell growth. Finally, using flow cytometry analysis we observed an increased number of apoptotic cells in QNC- and MBZ-treated A375 and M14 cells compared with vehicle-treated cells (Figure S3J).

To investigate the mechanisms underlying the pro-apoptotic responses triggered by QNC and MBZ, we analyzed the relative contribution of CASP-9 and -3–7 to QNC- and MBZ-mediated cell death using specific inhibitors. Our results revealed that melanoma cells become insensitive to both compounds in the presence of caspase inhibitors (Figures 3E–3H), suggesting that mitochondria-mediated apoptosis may be an important component of QNC- and MBZ-induced cell death.

We also tested their anti-tumor and pro-death efficacy in CASP9KO melanoma cells (Figures S4A and S4B). Results of CASP-3/7 and annexin V flow cytometry assays demonstrated a significant reduction in caspase-mediated cell death after QNC and MBZ treatments of A375-CASP9KO (Figures 3I and S4C–S4H). The sensitivity of both compounds was attenuated by CASP-9 suppression, as assessed by viability (Figure 3J) and colony-forming assays (Figures 3K and S4I), suggesting a mechanism of action dependent on CASP-9 activation.

Several reports showed that BCL-2 overexpression stabilizes mitochondria, preventing mitochondria-mediated apoptosis (Teijido and Dejean, 2010; Katoh et al., 2004). BCL-2 overexpression significantly decreased CASP-9 and -3/7 activity (Figures S4J–S4L) and reduced the number of apoptotic cells (Figures S4E, S4F, S4M, and S4N) in A375 cells treated with both drugs. Treatment with a QNC/MBZ combination did not significantly alter apoptosis in A375-CASP9KO (Figures 3I and S4E–S4H) and A375-BCL2 cells (Figures S4K–S4N). We observed a decreased efficacy in cell proliferation inhibition (Figures S4O and S4P), suggesting that the anti-tumor activity of QNC, MBZ, and their combination is mainly based on the induction of CASP-9-dependent mitochondrial apoptosis.

These findings showed that both QNC and MBZ efficiently suppressed tumor growth by inducing CASP-9- and mitochondrial-mediated apoptosis in melanoma cells, thus suggesting their potential for repurposing as therapeutic agents.

In vivo anti-tumor effects of QNC and MBZ

To study the *in vivo* efficacy of QNC and MBZ, xenografted melanoma models were generated, and QNC or MBZ were administered by peritoneal injection twice a week (Figure S4Q). The treatment was well tolerated, and treated mice showed no significant weight changes (Figures S4R and S4S).

Tumor growth was generally suppressed within the 33-day regimen (Figure 4A, 4D, 4E, S4X, and S4Y). A marked reduction in tumor volume was assessed at days 11 (beginning of treatment), and 22 and 33 (endpoint) in A375- and M14-xenografted mice treated with both QNC (Figures 4D, S4T, S4V, and S4X) and MBZ (Figures 4E, S4U, S4W, and S4Y). The median survival time of A375- and M14-xenografted treated mice is significant longer compared with controls (Figures 4B and 4C).

Melanoma growth suppression was further assessed by measuring Ki-67 levels in the A375- and M14-xenografted tumor masses (Figures 4F and S4Z). QNC and MBZ treatments significantly decrease the number of Ki-67-positive cells (Figures 4F and S4Z). Quantitative apoptotic rate comparison using anti-cleaved CASP-3 and -9 antibodies and TUNEL assay showed that both drugs more efficiently elicit apoptosis in A375 and M14 melanomas compared with controls (Figures 4F and S4Z).

These results strongly suggest that both drugs significantly induce apoptosis and suppress tumor growth *in vivo*.

QNC and MBZ suppress tumor growth in MAPKi-resistant melanoma cells

The clinical experience with MAPKi has shown that the efficacy of long-term treatment for melanoma patients is hampered by the development of resistance. It was important, therefore, to determine whether melanoma cells resistant to MAPKi remained sensitive to QNC and MBZ. We generated BRAF inhibitor- and MAPKi-resistant cells and compared the activities of QNC, MBZ, DABR, and TRAM in parental and resistant cells (Figures 5A, 5B, and S5A–S5J; Table S3). As expected, DABR and TRAM treatments resulted in dose-dependent cytotoxicity in the parental line, but had no effect on A375-BIR, M14-BIR, and A375-DR cells (Figures 5A, 5B, S5C–S5E, and S5H–S5J; Table S3). Conversely, QNC and MBZ retained full potency and anti-proliferative effect, irrespective of BRAFi resistance status (Figures S5A, S5B, S5F, and S5G; Table S3). Exposure of BRAFi-resistant cells to QNC or MBZ showed that these cells were more sensitive than the parental line, as indicated by their lower GI_{50} values (Table S3). Moreover, both compounds

(E and F) Analysis of CASP-9 activity in A375, M14 cells treated with QNC (E) and MBZ (F) alone or in combination with specific CASP-9 inhibitor Z-LEHD.
(G and H) Analysis of CASP-3/7 activity in A375, and M14 melanoma cells treated with QNC (G) and MBZ (H) alone or in combination with specific CASP-3/7 inhibitor Z-VAD-fmk.
(I) Analysis of CASP-3/7 activity in A375 and A375-CASP9KO cells treated with QNC (2 μM), MBZ (2 μM), and their combination for 8 and 48 h.
(J) Dose-response curves of A375 and A375-CASP9KO cells according to the sensitivity to QNC and MBZ. The mean GI_{50} values were 1.4 μM for QNC and 1.8 μM for MBZ in A375 cells, and 42 and 35 μM, respectively, in A375-CASP9KO.
(K) Colony-formation assays on A375 and A375-CASP9KO cells treated with QNC, MBZ, and DMSO. Representative images are presented. Statistical analyses were conducted by unpaired t test or one-way ANOVA. *$p < 0.01$, **$p < 0.001$, ***$p < 0.0001$, ****$p < 0.00001$; ns, not significant. Data are means ± SD of three independent experiments.

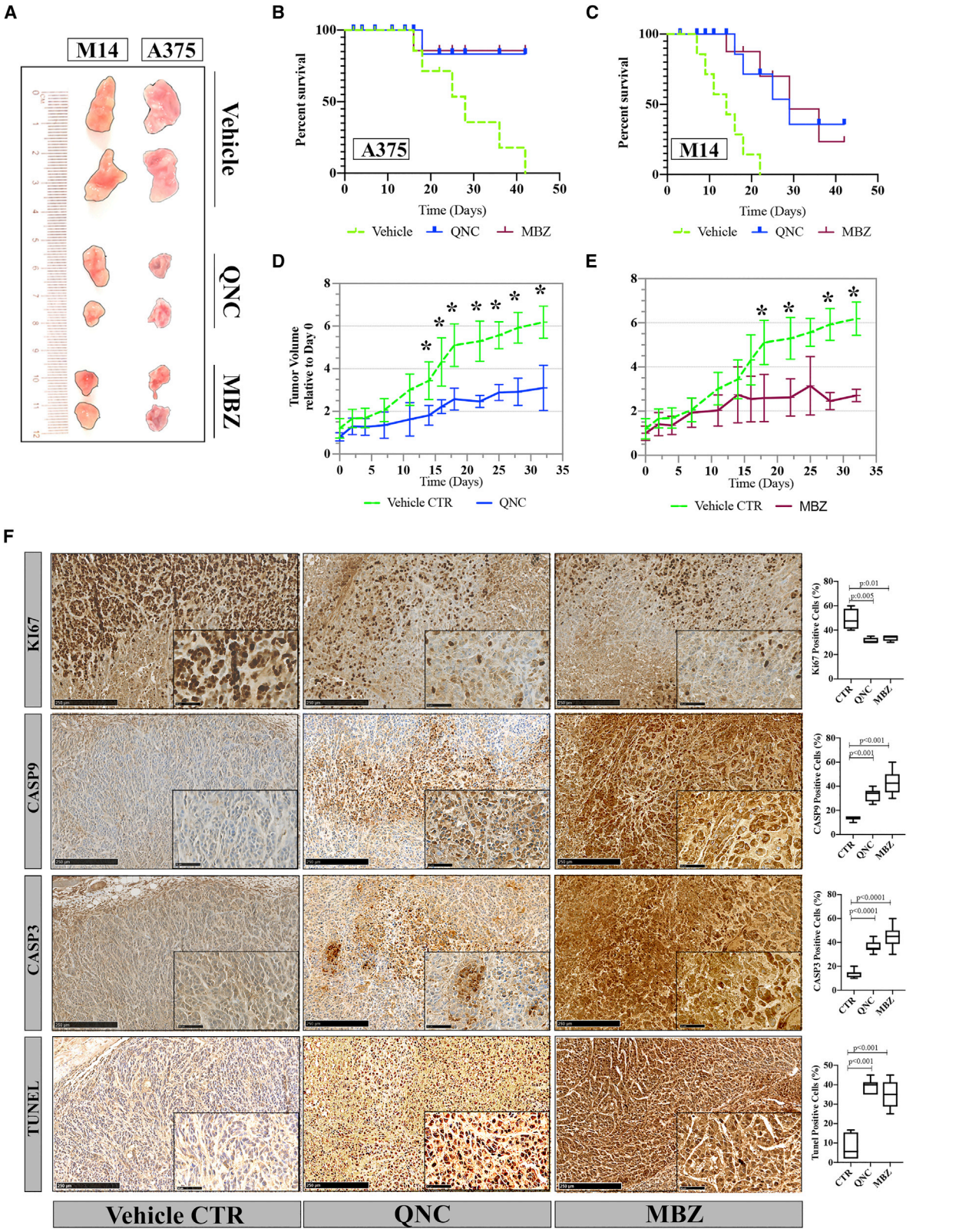

(legend on next page)

inhibited colony formation in drug-resistant cells (Figures 5C and S5K), while DABR treatment showed no inhibitory effects (Figures 5C and S5K).

Therefore, we investigated whether a combination of these drugs with MAPKi would be effective. Indeed, when QNC and MBZ were combined with DABR and TRAM, highly synergistic effects were scored at the concentrations tested, for the sensitive cells but importantly also for A375-BIR, M14-BIR, and A375-DR lines (Figures 5A and 5B; Table S3). Moreover, the combinatorial treatments effectively inhibited colony growth of A375-BIR and M14-BIR cells, thus enhancing the sensitivity of these cells to DABR (Figures 5C and S5K).

Next, we investigated if QNC, MBZ, and combinatorial treatments with MAPKi can induce apoptosis rather than slow proliferation in A375 and M14 parental and resistant cells (Figures S5L–S5O). Increased expression of cleaved CASP-9 and PARP clearly showed that QNC and MBZ treatments induce apoptosis in A374-BIR and M14-BIR cells (Figure S5L). Furthermore, immunoblot analysis with PARP, revealed that apoptosis is induced only when resistant cells are treated with DABR and TRAM in association with QNC and MBZ, respectively (Figure S5M). Using a CASP-3/7 activity assay we investigated the relative contribution of caspases to QNC- and MBZ-mediated apoptosis. While DABR and TRAM had no effect in triggering caspase activation in MAPKi-resistant cells, QNC and MBZ induced significant activation (Figure 5D). Moreover, combinatorial treatments of QNC/MBZ with MAPKi significantly re-sensitized cells to caspase-mediated apoptosis (Figure 5D). Using the CASP-3/7-specific inhibitor, we demonstrated that the pro-apoptotic effect is specifically mediated by the caspase-death pathway (Figure 5D). These results were confirmed by annexin V-FITC/PI fluorocytometry assay (Figures S5N–S5O).

Our findings indicate that QNC and MBZ exert anti-proliferative and pro-apoptotic effects in MAPKi-resistant melanoma cells. QNC and MBZ can re-sensitize resistant melanoma cells to MAPKi by triggering mitochondrial-mediated apoptosis, suggesting their potential use to overcome MAPKi resistance in melanoma.

QNC and MBZ increase sensitivity to dabrafenib in patient-derived melanoma cells

To determine the clinical relevance of our findings, we evaluated the efficacy of QNC and MBZ and combinatorial therapy with BRAFi in patient-derived cells with diverse genetic backgrounds established from different melanoma subtypes (Table S4).

We generated dose-response curves and GI_{50} values for QNC and MBZ treatments, showing that both drugs markedly suppressed cell viability in a dose-dependent manner (Figures 5E and 5F; Table S4). According to their DABR sensitivity, cells were categorized into DABR-sensitive and -resistant cells (Figures 5E and 5F). Combinatorial treatments (QNC or MBZ plus DABR) significantly reduced cell viability of patient-derived melanoma cells with respect to untreated controls or single drug treatments (Figures 5E, 5F, S5P, and S5R; Table S4).

Furthermore, QNC and MBZ significantly suppress colony formation in all patient-derived lines (Figures S5S and S5T), and their combination with DABR markedly inhibited colony formation in DABR-resistant cells (Figures S5S and S5T), providing further evidence that both drugs sensitize resistant cells to BRAF inhibitor treatment.

We demonstrated that MITF high/APAF1 low status correlates with MAPKi resistance (Figure 1). We evaluated the correlation between MITF/APAF1 expression ratio and the GI_{50} of DABR, DABR+QNC, and DABR+MBZ treatments (Figures S5P–S5R). As expected, significantly higher MITF/APAF1 ratios were observed in DABR-resistant cells (Figures S5P–S5R). We also observed elevated expression of MITF and MITF-related melanoma markers (TYR, MelanA, HMB45), concomitantly with low levels of APAF-1 in BRAFi-resistant cells (Figure S5U). The combination with QNC and MBZ significantly decreased the DABR GI_{50} (Figures S5P–S5R) in BRAFi-resistant cells, suggesting that QNC and MBZ may overcome the resistance induced by the MITF high/APAF1 low status.

Finally, to investigate if QNC and MBZ effectively overcome the resistance induced by different genetic profiles, we analyzed the sensitivity of QNC, MBZ, and combinations with DABR in relation to different mutational status of genes known to modulate drug sensitivity in melanoma (KRAS, NRAS, BRAF, TP53) (Figure 5G; Table S4). As expected, DABR sensitivity was strongly associated with genetic mutations in BRAF ($p < 0.001$). As previous reports showing that NRAS activation might induce acquired resistance to MAPKi in melanoma (Nazarian et al., 2010), we observed that resistant cells were wild type for BRAF and mutated in NRAS and TP53 (Figure 5G; Table S4). Interestingly, the association of DABR with QNC or MBZ significantly impacted the GI_{50} of DABR in resistant cells, restoring BRAFi sensitivity (Figures 5G and S5P).

These results demonstrate the anti-tumor efficacy of QNC, MBZ, and their combination with DABR in BRAF- and NRAS-mutated patient-derived melanoma cells compared with DABR alone, thus confirming their potential clinical relevance in the treatment of refractory melanomas.

QNC and MBZ treatments regulate the MITF network and other pivotal signaling pathways driving resistance in melanoma

To decipher the anti-tumor molecular mechanisms driven by QNC and MBZ, we investigated the transcriptome of A375-BIR, M14-BIR, and parental cells treated with the two drugs.

Figure 4. QNC and MBZ suppress melanoma growth in xenograft models

(A) Representative pictures of two explanted tumors per group.

(B and C) Survival of A375- (B) and M14- (C) xenografted mice is plotted as percentage of animals surviving/each group using a predefined cutoff volume of 1,000 mm^3 as surrogate for survival. Significance between groups was evaluated by the log rank (Mantel-Cox) test; $p < 0.05$).

(D and E) Efficacy data of QNC (D) and MBZ (E) are plotted as mean tumor volume (mm^3) ± SD normalized to baseline pre-treatment tumor size (D0). *$p < 0.05$.

(F) Histological sections of control, QNC- and MBZ-treated A375-xenografted tumors, stained with Ki-67, CASP-9, CASP-3, and Tunnel. Bars showing average percentages of positive cells are presented on the right. Scale bar, 100 μm. Student's t test showing statistically significant difference between the groups (n = 15). *$p < 0.01$.

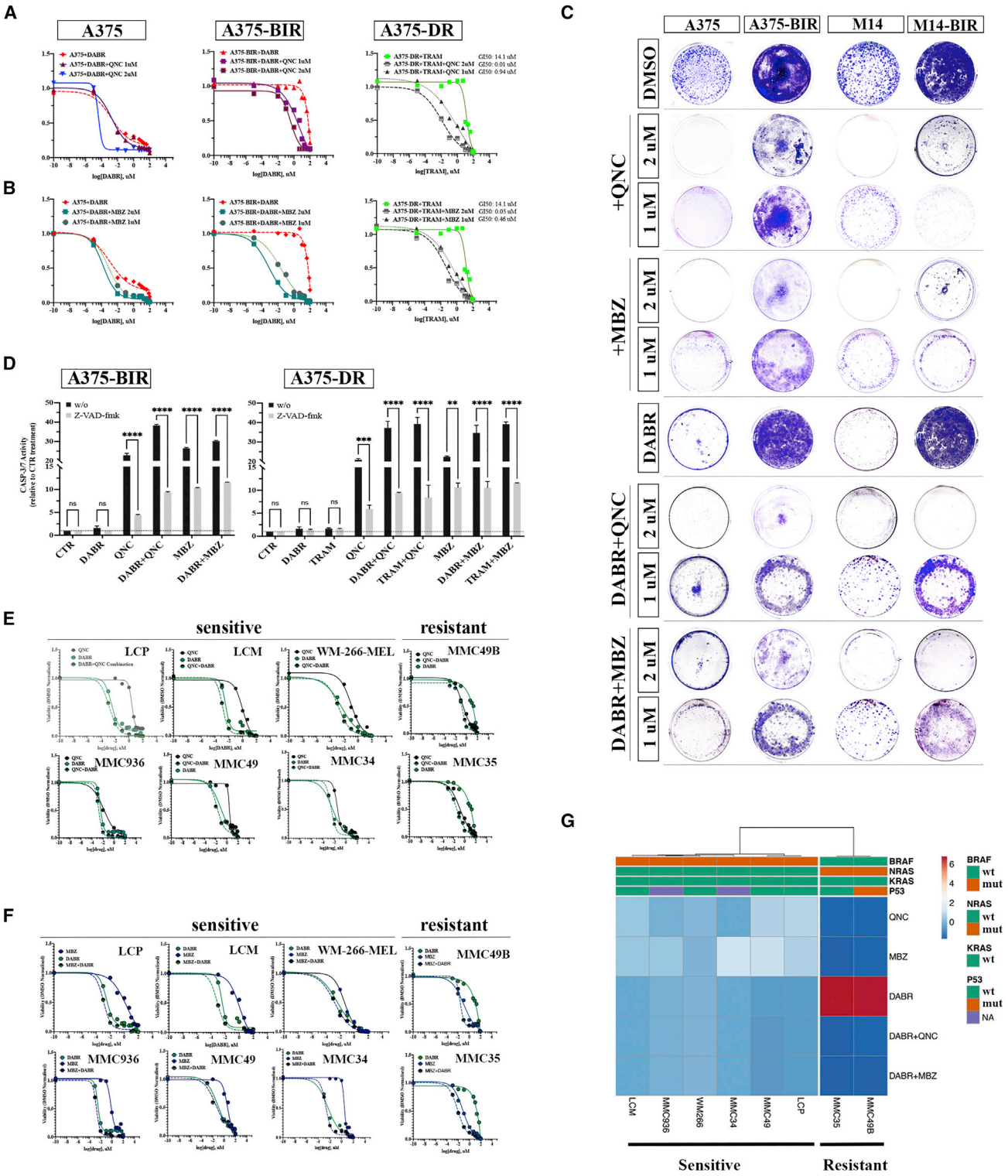

Figure 5. QNC and MBZ sensitize melanoma-resistant cells to MAPKi

(A and B) Dose-response curves of MAPKi-resistant A375-BIR, A375-DR melanoma cells, and parental cell lines, according to sensitivity to QNC, MBZ, DABR, and TRAM and their combinations.

(C) Colony-formation assays of A375-BIR and M14-BIR melanoma cells and parental cell lines treated with DABR alone or in combination with QNC or MBZ and DMSO.

(legend continued on next page)

The analysis of RNA-seq data revealed substantial changes when comparing QNC- or MBZ-treated with vehicle-treated cells (Figures 6A, 6B, S6A, and S6B). Differentially regulated transcripts in each group are highlighted by a Venn diagram (Figures S6C–S6F).

GSEA was performed using the Hallmark and Biocarta gene set collections in the Molecular Signatures Database (MSigDB). Gene sets related to cell cycle, cell growth, and melanoma-related pathways were significantly downregulated by both drugs in parental and resistant cells (G2M-Checkpoint, E2F-targets, Mitotic-Spindle, MYC-Targets; PI3K/AKT/MTOR; Hypoxia; MAPK; Figures 6E and S6G; Table S5). Cell-death-related gene sets were among the top ranked for upregulation gene sets (e.g., apoptosis, BAD, mitochondria, and P53 death pathways) (Figures 6C–6F, S6G, and S6H; Table S5). Interestingly, gene sets related to oncogenic pathways (e.g., angiogenesis, KRAS, Hystone De-acetylase, RHO, and MAPK) were negatively correlated to QNC or MBZ treatments (Figures 6C–6F, S6G, and S6H; Table S5).

We examined the impact of QNC and MBZ treatments on MITF-regulated transcriptional network, a key driver of melanoma-genesis, and BRAFi resistance (Smith et al., 2016). GSEA using a custom gene set (Möller et al., 2019a) showed significant inhibition of the MITF transcriptional program in resistant and parental cells treated with both drugs (Figures 6E and 6F; Table S5).

MITF plays a role in the transcriptional regulation of lysosomal and autophagosomal genes (Möller et al., 2019a). Our results revealed significant downregulation of MITF-related transcription factors and lyso-autophagy gene sets, suggesting that QNC and MBZ may inhibit lyso-autophagy through transcriptional inhibition of the MITF network (Figurse 6E, 6F, and S6I–S6L). RT-PCR analysis showed that several genes of this network regulating lyso-autophagy, were significantly decreased by both drugs (Figures S6K and S6L).

We also studied the inhibitory functional effect of QNC and MBZ on the MITF pathway in tumors isolated from xenografted mice. IHC analysis clearly showed a reduction of MITF and MLANA (an MITF target gene) expression and of the number of positive cells in both A375- and M14-xenografted tumors treated with QNC and MBZ (Figures 6G and 6H). These data strongly suggest that both drugs suppress the MITF transcriptional network and therefore tumor growth in melanoma *in vivo* models.

We next investigated functional effects of both drugs on lyso-autophagy. We used a fluorescently tagged-LC3 reporter assay to study the mechanisms regulating autophagosome maturation (Morleo et al., 2021). Confocal microscopy analysis revealed a significant difference in the total number of LC3 puncta (yellow) in cells treated with QNC and MBZ, in comparison with control-treated cells (Figure 6I). Interestingly, QNC was a more potent lyso-autophagy inhibitor than CQ (Figure 6I). We also observed a marked increase of LC3-II when A375 and A375-BIR cells were exposed to both QNC and MBZ, clearly indicating an autophagic flux blockade (Figures S6M–S6P). These results were confirmed by immunofluorescent LC3-II staining (Figure S6Q).

These findings suggest that the modulation of different gene networks by QNC and MBZ contribute to reverse BRAFi resistance; in particular, MITF function is markedly suppressed in melanoma cells and in xenografted tumors.

QNC and MBZ overcome MITF/APAF-1-mediated resistance by targeting HDAC

Our data suggested that the MITF/APAF-1 axis is involved in driving MAPKi resistance in melanoma.

We designed *in vitro* assays to evaluate whether QNC and MBZ may overcome MAPKi resistance by targeting the MITF/APAF-1 axis. Depletion of APAF-1 from A375 cells and overexpression of MITF significantly impacted the resistance to DABR and TRAM treatment, increasing the GI_{50} with respect to control-treated cells (Figures 1L, 1M, 7A, and 7B; Table S6). Dose-response analysis also showed that, both in APAF-1-depleted and MITF-overexpressing A375 cells, the combination of QNC or MBZ with DABR or TRAM reduced the GI_{50} by ~1,000-fold compared with treatments with single agents (Figures 7A and 7B; Table S6).

Consistent with these observations, RNAi-mediated APAF-1 depletion in A375 cells antagonized the pro-apoptotic effect of MAPKi treatment as detected by decreased PARP-1 and CASP-3 cleavage in immunoblotting (Figures S7A and S7B). APAF-1 depletion did not affect the ERK1/2 pathway inhibition, as assessed by undetectable levels of phosphorylated ERK1/2 (p-ERK1/2). Conversely, QNC or MBZ treatments combined with MAPKi, re-sensitized cells to MAPKi, as revealed by increased levels of apoptotic markers (Figures S7A and S7B). Moreover, ectopic overexpression of MITF in A375 cells reduced expression of both APAF-1 (Figures S7C and S7J) and apoptotic markers (PARP-1 and CASP-3) in MAPKi-treated cells (Figures S7C and S7D), confirming that MITF may drive resistance to MAPKi by preventing the apoptosis program. In MITF-overexpressing A375 cells, MAPKi treatment did not affect p-ERK1/2 levels, indicating that MITF confers MAPKi resistance by re-wiring ERK1/2 signaling (Figure S7C). The levels of apoptotic marker expression were restored by simultaneous treatment with QNC or MBZ (Figures S7C and S7D), indicating that these drugs may re-sensitize MITF-overexpressing cells to apoptosis. ERK1/2 pathway inhibition is strongly marked in MITF-overexpressing cells treated with QNC or MBZ in combination with MAPKi (Figures S7C and S7D), thus confirming their synergistic effect in inhibiting the MITF-BRAF-MAPK pathway.

(D) Analysis of CASP-3/7 activity in A375-BIR, A375-DR cells treated with QNC, MBZ, and their combination with DABR and TRAM with or without the CASP-3/7 inhibitor Z-VAD-fmk.

(E and F) Dose-response curves of patient-derived melanoma cells according to their sensitivity to QNC (E), MBZ (F), and DABR.

(G) Associations between sensitivity to QNC, MBZ, DABR, and their combinations with selected genetic alterations in patient-derived melanoma cell lines. Hierarchical clustering is based on the Euclidian distance calculated with an average linkage clustering algorithm. The color coding was scaled separately for each row to demonstrate GI_{50} differences (mut, mutated; wt, wild type; NA, not assessed). Data are means ± SD of three independent experiments. Statistical analyses were conducted by unpaired t test or one-way ANOVA. *$p < 0.01$, **$p < 0.001$, ***$p < 0.0001$, ****$p < 0.00001$; ns, not significant.

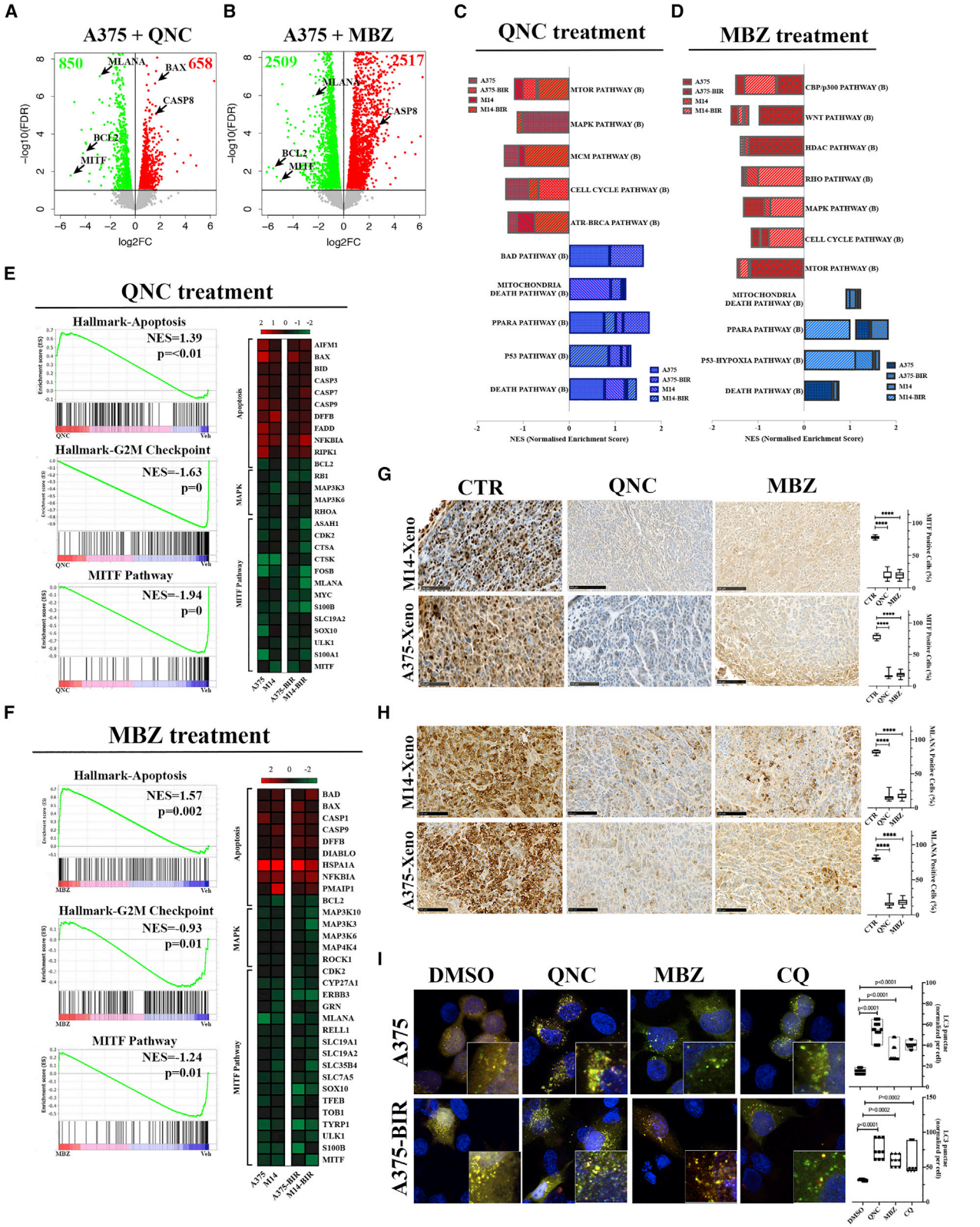

(legend on next page)

We demonstrated that QNC and MBZ treatments induced downregulation of MITF and its gene network in DABR-resistant melanoma cells (Figures 6 and S6). We next aimed to verify if QNC and MBZ affect MITF expression in a larger panel of melanoma cells. MITF mRNA levels were reduced by both QNC (Figures S7E–S7G) and MBZ (Figures S7F–S7H) treatment.

We performed a functional viability-based screening to assess the relevance of the MITF/APAF-1 axis in establishing MAPKi resistance. In parallel we evaluated the efficacy of QNC and MBZ in sensitizing cells to MAPKi by targeting the MITF/APAF-1 axis. We therefore tested MAPKi sensitivity of melanoma cells simultaneously silenced for APAF-1 or overexpressing MITF (Figures 7C and S1J). Interestingly, the overexpression of MITF induced downregulation of APAF-1 (Figure S1J). As expected, the treatment with MAPKi did not reduce cell viability (Figure 7C), while the combination with QNC or MBZ restored MAPKi sensitivity (Figure 7C). GI_{50} analysis across all cell lines revealed that the combined treatments of QNC or MBZ with MAPKi efficiently reduced the MAPKi GI_{50} in cells with MITF high/APAF-1 low transcriptional status (Figure 7D). These findings demonstrate that QNC or MBZ efficiently surpassed MAPKi resistance by efficiently targeting the MITF/APAF-1 axis.

To investigate the mechanism of action of QNC and MBZ, we designed an *in silico* virtual screening followed by *in vitro* validation to identify novel targets potentially regulating MITF/APAF-1 transcriptional status. A computational screening based on two chemoinformatic tools (MANTRA [Iorio et al., 2010]; SwissTargetPrediction [Daina et al., 2019]) identified the histone deacetylases (HDACs) as potential target class of QNC and MBZ (see STAR methods). Notably, epigenetic regulation of MITF expression through HDACs has been described (Yokoyama et al., 2008).

We therefore measured HDAC inhibitory activity of both drugs in A375-DR cells, observing that QNC more potently inhibits HDAC class I and II activities with respect to other classes, while MBZ showed higher activity against HDAC class IV/Sirtuins (SIRTs; Figure S7J). QNC and MBZ showed also higher potency in inhibiting HDAC class I/II and Sirtuins, respectively, than trichostatin or Sirtinol (SIRT) (Figure S7K). Moreover, the acetylation status of histone H3 in A375-DR cells correlated with activity of both drugs and with the MITF suppression (Figure S7L), thus confirming that both compounds can inhibit HDAC activity. QNC and MBZ were further profiled for isoform selectivity with a panel of fluorogenic assays against HDAC class I, II, and SIRT isoforms (Figure 7E). QNC showed higher potency against HDAC6 and 8, while MBZ showed higher potency against SIRT5 (Figure 7E). To confirm that QNC and MBZ suppress MITF expression via specific isoforms, HDAC6, 8, and SIRT5 were knocked down by siRNA. Significant changes of MITF and APAF-1 levels were detected by RT-PCR in A375-DR cells depleted for HDAC isoforms, showing that HDAC6/8 and SIRT5 are key players in epigenetic regulation of MITF and APAF-1 (Figure S7M). Interestingly, silencing HDAC6, 8, or both, in A375-DR cells attenuated QNC-mediated suppression of MITF, suggesting that both HDACs play a key role in QNC-mediated MITF suppression (Figure S7N). However, MBZ-mediated MITF suppression was attenuated in cells silenced for SIRT5, thus identifying SIRT5 as the main MBZ target in epigenetic regulation of MITF (Figure S7O).

These findings show the mechanistic model by which QNC and MBZ may efficiently overcome MAPKi resistance by epigenetically suppressing MITF expression (Figures 7F and 7G) and represent the rationale for the use of these drugs in MAPKi-resistant melanomas.

DISCUSSION

The ability of cancer cells to evade apoptosis is considered a "hallmark of cancer" conferring cancer cells survival and their resistance to therapeutic agents (Hanahan and Weinberg, 2000). Strategies overcoming or bypassing the inhibition of apoptosis may provide therapeutic options for resistant cancers. The observation that key components of the apoptosome, such as APAF-1 and CASP-9, are frequently silenced or inactivated in human cancer supports this statement. APAF-1-inactivation was first reported in metastatic melanomas (Soengas and Lowe, 2003; Soengas et al., 2001; Fujimoto et al., 2004) and it has been shown that loss of APAF-1 may contribute to chemoresistance in melanoma (Dai et al., 2004; Zanon et al., 2004) and other cancers (Umetani et al., 2004; Zlobec et al., 2007). However, this concept is disputed by *in vitro* studies (van Allen et al., 2015; Peltenburg et al., 2005; Zanon et al., 2004). Our study focused on the role of APAF-1 in resistance to current therapeutic regimens and combines patient-derived data and cellular models. This complete context allowed evaluation of the functional correlation between APAF-1 inactivation and MAPKi resistance in melanoma. By analyzing the transcriptome profiles of two independent cohorts of BRAF-mutated metastatic melanoma patients

Figure 6. Effects of QNC and MBZ on global gene expression in melanoma cells

(A and B) Volcano plots displaying upregulated (red) and downregulated (green) genes after QNC (A) and MBZ (B) treatment in A375 cells (adjusted-log10(FDR) versus log2 fold change). Example of differentially expressed (DE) genes indicated by a black arrow.

(C and D) Plot of functional GSEA indicating pathways significantly modulated by QNC (C) and MBZ (D) treatment in A375, A375-BIR, M14, and M14-BIR cells; red and blue bars represent, respectively, down- and upregulated gene sets ($p = 0.05$).

(E and F) Representative enrichment plots of selected gene sets in cells treated with QNC (E) and MBZ (F) in comparison with DMSO-treated controls. Normalized enrichment score (NES) and FDRs are shown for each gene set (FDR < 0.05). Representative heatmaps of DE genes constituting the leading-edge subsets within the gene sets shown, respectively, in QNC- and MBZ-treated cells. Each row represents a gene, and each column represents the fold change (log) of QNC-treated (E) and MBZ-treated (F) cells versus DMSO-treated controls.

(G and H) Histological sections of control (CTR), QNC- and MBZ-treated A375- and M14-xenografted tumors stained with MITF (G) and MLANA (H). Scale bar, 100 μm. Bars showing average percentages of positive cells are presented on the right (****$p < 0.001$; $n = 15$).

(I) Blockade of autophagic flux in A375 and A375BIR cells treated with DMSO, QNC, MBZ, or CQ. Representative merged images of red and green channels are shown. Original magnification, 40×. Scale bars, 50 μm. Blockade of autophagic flux (measured by yellow puncta) was quantified (mean ± SD of triplicate experiments). Statistical analyses were conducted by unpaired t test or one-way ANOVA. *$p < 0.01$, **$p < 0.001$, ***$p < 0.0001$, ****$p < 0.00001$; ns, not significant.

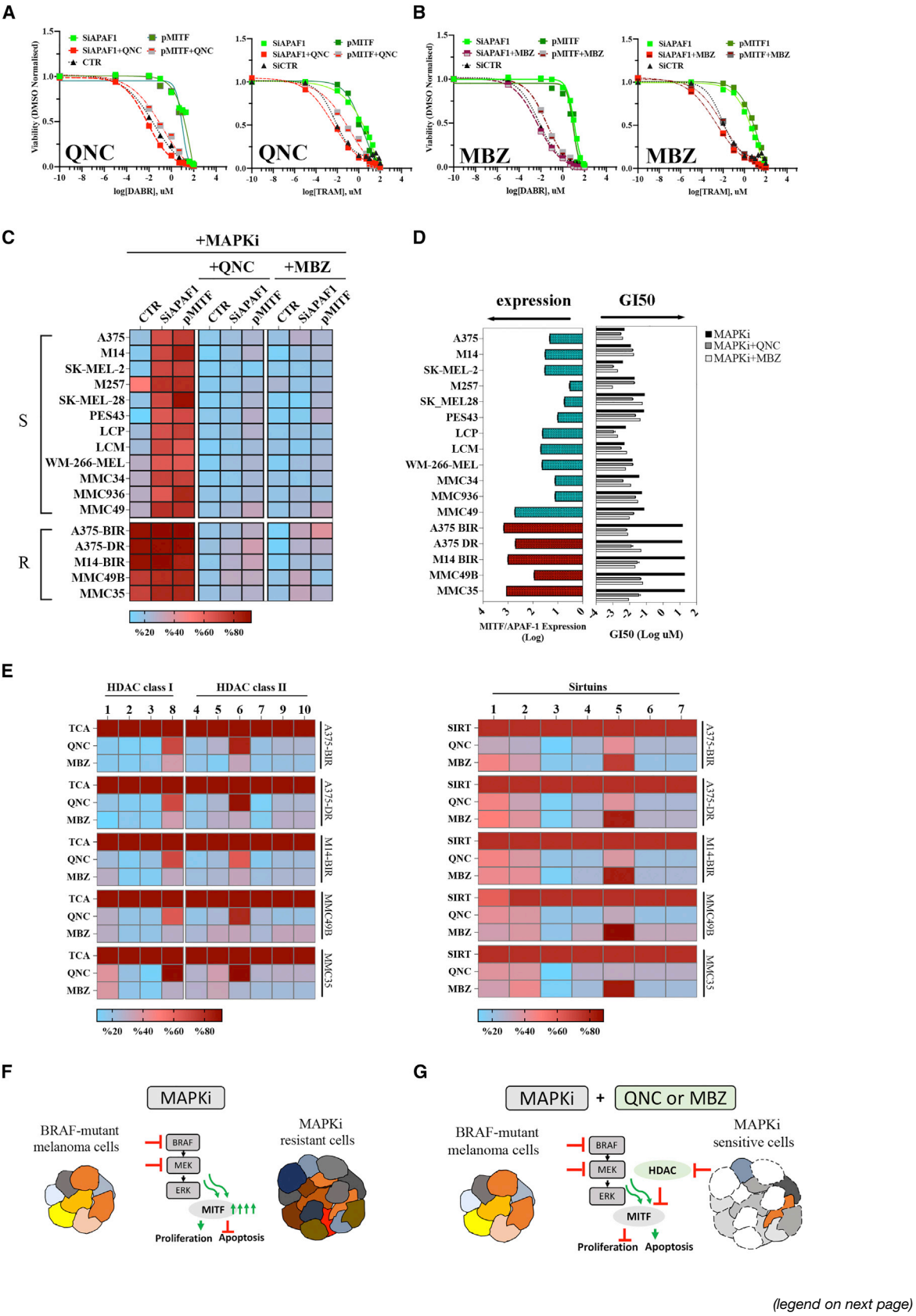

(legend on next page)

we found low levels of APAF-1 expression strongly correlated with increased MITF expression in patients with the worse clinical responses to MAPKi. We demonstrated for the first time that the MITF/APAF-1 axis markedly modulates MAPKi sensitivity and resistance. Enhanced MITF expression or amplification is linked to innate or acquired resistance in melanoma (Smith et al., 2016; Wellbrock and Arozarena, 2015). In line with these reports, our findings provided evidence that MITF can drive MAPKi resistance through various mechanisms, such as enhancing survival signaling, inhibiting apoptosis, and altering metabolism. We thus reasoned that the MITF/APAF-1 pathway may be an intrinsic or acquired mechanism to protect melanoma cells from drug-induced death, and that APAF-1 might constitute a melanoma-specific therapeutic target. To evaluate this possibility, a drug-repositioning screening strategy was designed to identify agents specifically inducing apoptosis independently of apoptosome function. This strategy allowed us to perform a screening in a context mimicking the biology of drug resistance. We identified two compounds (QNC and MBZ), which selectively activate apoptosome-independent cell death. The mechanism of action used by QNC and MBZ has been clearly elucidated, showing that both drugs exert their anti-tumor activity by causing CASP-9-mediated cell death and mitochondrial apoptosis. Alternative mechanisms for caspase activation exist independently of APAF-1 (Manns et al., 2011; Rao et al., 2002; Belmokhtar et al., 2003; Imao and Nagata, 2013; Indrieri et al., 2013). Our results first suggested a functional association between this non-canonical mitochondrial apoptotic pathway and MAPKi resistance in melanoma. Further experiments are required to understand if the non-canonical APAF-1 independent pathway works preferentially in cell types with intrinsic or acquired drug resistance. Moreover, we found that both QNC and MBZ profoundly sensitize *BRAF* and *NRAS* mutant melanoma cells resistant to MAPKi and are effective in reversing the resistance in melanoma cells isolated from patients.

We demonstrated that QNC and MBZ target the MITF/APAF-1 pathway by negatively regulating MITF and the MITF-related gene networks, commonly recognized as drivers of oncogenesis and drug resistance in melanoma (Möller et al., 2019a; Wang et al., 2018). QNC is a well-known drug, reported to induce apoptosis and block proliferation in several solid (Mohapatra et al., 2012; Das et al., 2017; Gurova et al., 2005) and hematopoietic (Eriksson et al., 2015) cancers. Analysis of the signaling pathways involved in QNC-mediated apoptosis highlighted QNC as an efficient modulator of PI3K/AKT/mTOR signaling and the companion gene networks MITF and P53 in MAPKi-resistant melanoma cells.

MBZ is a synthetic compound identified in a drug screening on drug-resistant colon cancer cells (Pellegrini et al., 2018). In line with previous observations (Huang et al., 2019), we found that MBZ negatively modulated MAPK, RHO, and cell-cycle-related pathways. Considering that melanomas often exhibit increased ERK-MAPK activity (Lopez-Bergami et al., 2007), MBZ may be proposed to target MAPK in resistant melanoma, where other strategies fail.

We have for the first time identified and validated QNC and MBZ as epigenetic inhibitors of MITF. We demonstrated that their potency in suppressing MITF expression is caused by targeting specific HDAC isoforms. Notably, the pharmacologic suppression of MITF by the HDAC inhibitor (HDACi) has been reported (Yokoyama et al., 2008) and several HDACi were found to overcome resistance in melanoma (Emmons et al., 2019).

Repurposing QNC and MBZ as anticancer agents may be a promising strategy due to their ability to target multiple pathways, and their synergistic cytotoxicity when combined with other anticancer agents. In conclusion, our results identify a new and unexpected function for MITF/APAF-1 signaling in resistant melanoma and identify a potential clinically actionable strategy to overcome MAPKi resistance.

STAR★METHODS

Detailed methods are provided in the online version of this paper and include the following:

- KEY RESOURCES TABLE
- RESOURCE AVAILABILITY
  - Lead contact
  - Materials availability
  - Data and code availability
- EXPERIMENTAL MODEL AND SUBJECT DETAILS
  - Patient samples
  - Cell lines and patient-derived cells
- METHOD DETAILS
  - Transfection
  - Generation of CASP9 gene knockout in A375 cells
  - High-throughput compound screening
  - Caspase activity assay
  - Western blot analysis
  - Quantitative real-time PCR analysis
  - Proliferation assay
  - Colony formation assay
  - Annexin V-FITC/PI staining assay
  - Animal studies

Figure 7. QNC and MBZ increase the sensitivity of melanoma cells to MAPKi by targeting the MITF/APAF-1 axis

(A and B) Dose-response curves (mean ± SEM) for DABR and TRAM in the presence of QNC (A) and MBZ (B) in A375 cells, transfected with CTRs, MITF-expressing vector (pMITF), or APAF-1-specific siRNAs (SiAPAF1).

(C and D) Survival profile of melanoma cells transfected with SiAPAF1, pMITF, and relative CTRs, followed by treatment with MAPKi (DABR plus TRAM) in combination with QNC or MBZ.

(D) Melanoma cells were grouped based on MITF/APAF-1 expression and sensitivity (GI_{50}) to treatments with MAPKi and their combinations with QNC or MBZ (Table S6). Red and blue bars represent MAPKi-resistant (R) and -sensitive (S) cell lines, respectively.

(E) Biochemical profiling of isoform selectivity of HDAC inhibitor hits. TCA, SIRT, QNC, and MBZ were tested with individual recombinant HDAC class enzymes and their corresponding fluorogenic substrates. Efficacy values were averaged from three replicates and shown in heat map.

(F and G) MITF activates a network of genes, which in turn increases cell proliferation and inhibits the apoptotic programs (F). In resistant melanomas QNC and MBZ suppress cell proliferation and activate apoptosis by targeting specific HDACs that negatively regulate MITF expression (G).

SUPPLEMENTAL INFORMATION

Supplemental information can be found online at https://doi.org/10.1016/j.celrep.2022.111601.

ACKNOWLEDGMENTS

This study was supported by POR CAMPANIA FESR 2014/2020 grant (CUP B61G18000470007) and by the Italian Association for Cancer Research (AIRC) (IG 17711/2015; 26414/2022 to B.F.). P.C. is the recipient of a Marie Skłodowska-Curie Career Re-Integration fellowship funded by the AIRC and the EU Horizon 2020 programme (grant 800924). We thank Dr. J. Monfregola for CRISPR-CAS9 gene editing. We thank the High Content Screening (HCS) facility and the Bioinformatics Core at Tigem for technical support.

AUTHOR CONTRIBUTIONS

Study concept and design, P.C., B.F., A.R., and A. Indrieri; data acquisition, A. Barbato, P.C., A.R., A. Iuliano, A. Barbieri, C.A., P.Q., M.V., S.B., L.F., R.D.C., M.M., M.C., G.M., E.C., and R.T.; data analysis/interpretation, P.C., B.F., A. Indrieri, A.R., R.D., E.C., G.T., P.A.A., A. Iuliano, and R.D.C.; drafting of the manuscript, P.C. and B.F.; intellectual contribution, P.C., B.F., P.A.A., G.T., A.R., and A. Indrieri; statistical analysis, A. Iuliano and P.C.; material support, A. Barbato, A. Barbieri, C.A., P.Q., M.V., S.B., L.F., R.D.C., M.M., M.C., G.M., L.L., E.C., A.R., R.T., M.T., and F.T.; funding, P.C. and B.F.

DECLARATION OF INTERESTS

P.A.A. reports grants and/or personal fees from BMS, Roche-Genentech and Array, MSD, Novartis, Merck Serono, Pierre Fabre, Incyte, Genmab, NewLink Genetics, Medimmune, AstraZeneca, Syndax, Sun Pharma, Sanofi, Idera, Ultimovacs, Sandoz, Immunocore, 4SC, Alkermes, and Nektar, Italfarmaco, outside the submitted work. All other authors declare no competing interests.

Received: July 6, 2021
Revised: February 9, 2022
Accepted: October 13, 2022
Published: November 8, 2022

REFERENCES

Andreu-Fernández, V., Genovés, A., Messeguer, A., Orzáez, M., Sancho, M., and Pérez-Payá, E. (2013). BH3-Mimetics- and cisplatin-induced cell death proceeds through different pathways depending on the availability of death-related cellular components. PLoS One *8*, e56881. https://doi.org/10.1371/journal.pone.0056881.

Barbato, A., Iuliano, A., Volpe, M., D'alterio, R., Brillante, S., Massa, F., De Cegli, R., Carrella, S., Salati, M., Russo, A., et al. (2021). Integrated genomics identifies MiR-181/TFAM pathway as a critical driver of drug resistance in melanoma. Int. J. Mol. Sci. *22*, 1801. https://doi.org/10.3390/ijms22041801.

Belmokhtar, C.A., Hillion, J., Dudognon, C., Fiorentino, S., Flexor, M., Lanotte, M., and Ségal-Bendirdjian, E. (2003). Apoptosome-independent pathway for apoptosis. J. Biol. Chem. *278*, 29571–29580. https://doi.org/10.1074/jbc.M302924200.

Buchser, W., Collins, M., Garyantes, T., Guha, R., Haney, S., Lemmon, V., Li, Z., and Trask, O.J. (2014). Assay development guidelines for image-based high content screening, high content analysis and high content imaging. Assay Guidance Manual.

Carotenuto, P., Amato, F., Lampis, A., Rae, C., Hedayat, S., Previdi, M.C., Zito, D., Raj, M., Guzzardo, V., Sclafani, F., et al. (2021). Modulation of pancreatic cancer cell sensitivity to FOLFIRINOX through microRNA-mediated regulation of DNA damage. Nat Commun *12*, 6738. https://doi.org/10.1038/s41467-021-27099-6.

Carotenuto, P., Hedayat, S., Fassan, M., Cardinale, V., Lampis, A., Guzzardo, V., Vicentini, C., Scarpa, A., Cascione, L., Costantini, D., et al. (2020). Modulation of biliary cancer chemo-resistance through MicroRNA-mediated rewiring of the expansion of CD133+ cells. Hepatology *72*, 982–996. https://doi.org/10.1002/hep.31094.

Cecconi, F., Alvarez-Bolado, G., Meyer, B.I., Roth, K.A., and Gruss, P. (1998). Apaf1 (CED-4 homolog) regulates programmed cell death in mammalian development. Cell *94*, 727–737. https://doi.org/10.1016/S0092-8674(00)81732-8.

Dai, D.L., Martinka, M., Bush, J.A., and Li, G. (2004). Reduced Apaf-1 expression in human cutaneous melanomas. Br. J. Cancer *91*, 1089–1095. https://doi.org/10.1038/sj.bjc.6602092.

Daina, A., Michielin, O., and Zoete, V. (2019). SwissTargetPrediction: updated data and new features for efficient prediction of protein targets of small molecules. Nucleic Acids Res. *47*, 357–364. https://doi.org/10.1093/nar/gkz382.

Das, S., Nayak, A., Siddharth, S., Nayak, D., Narayan, S., and Kundu, C.N. (2017). TRAIL enhances quinacrine-mediated apoptosis in breast cancer cells through induction of autophagy via modulation of p21 and DR5 interactions. Cell. Oncol. *40*, 593–607. https://doi.org/10.1007/s13402-017-0347-3.

Edgar, R., Domrachev, M., and Lash, A.E. (2002). Gene Expression Omnibus: NCBI gene expression and hybridization array data repository. Nucleic Acids Res. *30*, 207–210. https://doi.org/10.1093/nar/30.1.207.

Elgendy, M., Ciro, M., Abdel-Aziz, A.K., Belmonte, G., Dal Zuffo, R., Mercurio, C., Miracco, C., Lanfrancone, L., Foiani, M., and Minucci, S. (2014). Beclin 1 restrains tumorigenesis through Mcl-1 destabilization in an autophagy-independent reciprocal manner. Nat Commun, 5. https://doi.org/10.1038/ncomms6637.

Elgendy, M., Cirò, M., Hosseini, A., Weiszmann, J., Mazzarella, L., Ferrari, E., Cazzoli, R., Curigliano, G., DeCensi, A., Bonanni, B., et al. (2019). Combination of Hypoglycemia and Metformin Impairs Tumor Metabolic Plasticity and Growth by Modulating the PP2A-GSK3β-MCL-1 Axis. Cancer Cell *35*, 798–815.e5. https://doi.org/10.1016/j.ccell.2019.03.007.

Emmons, M.F., Fai∼ Ao-Flores, F., Sharma, R., Thapa, R., Messina, J.L., Becker, J.C., Schadendorf, D., Seto, E., Sondak, V.K., Koomen, J.M., et al. (2019). HDAC8 regulates a stress response pathway in melanoma to mediate escape from BRAF inhibitor therapy. Cancer Res. *79*, 2947–2961. https://doi.org/10.1158/0008-5472.CAN-19-0040.

Eriksson, A., Österroos, A., Hassan, S., Gullbo, J., Rickardson, L., Jarvius, M., Nygren, P., Fryknäs, M., Höglund, M., and Larsson, R. (2015). Drug screen in patient cells suggests quinacrine to be repositioned for treatment of acute myeloid leukemia. Blood Cancer J. *5*, e307. https://doi.org/10.1038/bcj.2015.31.

Fischer, G.M., Vashisht Gopal, Y.N., McQuade, J.L., Peng, W., DeBerardinis, R.J., and Davies, M.A. (2018). Metabolic strategies of melanoma cells: mechanisms, interactions with the tumor microenvironment, and therapeutic implications. Pigment Cell Melanoma Res. *31*, 11–30. https://doi.org/10.1111/pcmr.12661.

Frederick, D.T., Piris, A., Cogdill, A.P., Cooper, Z.A., Lezcano, C., Ferrone, C.R., Mitra, D., Boni, A., Newton, L.P., Liu, C., et al. (2013). Cancer therapy: clinical BRAF inhibition is associated with enhanced melanoma antigen expression and a more favorable tumor microenvironment in patients with metastatic melanoma. Clin. Cancer Res. *19*, 1225–1231. https://doi.org/10.1158/1078-0432.CCR-12-1630.

Fujimoto, A., Takeuchi, H., Taback, B., Hsueh, E.C., Elashoff, D., Morton, D.L., and Hoon, D.S.B. (2004). Allelic imbalance of 12q22-23 associated with

APAF-1 locus correlates with poor disease outcome in cutaneous melanoma. Cancer Res. *64*, 2245–2250. https://doi.org/10.1158/0008-5472.CAN-03-2932.

Furukawa, Y., Sutheesophon, K., Wada, T., Nishimura, M., Saito, Y., Ishii, H., and Furukawa, Y. (2005). Methylation Silencing of the Apaf-1 Gene in Acute Leukemia. Mol. Cancer Res. *3*, 325–334.

Gentilcore, G., Madonna, G., Mozzillo, N., Ribas, A., Cossu, A., Palmieri, G., and Ascierto, P.A. (2013). Effect of dabrafenib on melanoma cell lines harbouring the BRAFV600D/R mutations. BMC Cancer *13*, 17. https://doi.org/10.1186/1471-2407-13-17.

Gurova, K.v., Hill, J.E., Guo, C., Prokvolit, A., Burdelya, L.G., Samoylova, E., Khodyakova, A.v., Ganapathi, R., Ganapathi, M., Tararova, N.D., et al. (2005). Small molecules that reactivate p53 in renal cell carcinoma reveal a NF-κB-dependent mechanism of p53 suppression in tumors. Proc. Natl. Acad. Sci. USA *102*, 17448–17453. https://doi.org/10.1073/pnas.0508888102.

Hanahan, D., and Weinberg, R.A. (2000). The hallmarks of cancer review douglas. Cell *100*, 57–70.

Hinz, S., Kempkensteffen, C., Weikert, S., Schostak, M., Schrader, M., Miller, K., and Christoph, F. (2007). EZH2 polycomb transcriptional repressor expression correlates with methylation of the APAF-1 gene in superficial transitional cell carcinoma of the bladder. Tumour Biol. *28*, 151–157. https://doi.org/10.1159/000103380.

Huang, X.-H., Wang, Y., Hong, P., Yang, J., Zheng, C.-C., Yin, X.-F., Song, W.-B., Xu, W.W., Li, B., and He, Q.-Y. (2019). Benzethonium chloride suppresses lung cancer tumorigenesis through inducing p38-mediated cyclin D1 degradation. Am. J. Cancer Res. *9*, 2397–2412.

Imao, T., and Nagata, S. (2013). Apaf-1- and caspase-8-independent apoptosis. Cell Death Differ. *20*, 343–352. https://doi.org/10.1038/cdd.2012.149.

Indrieri, A., Conte, I., Chesi, G., Romano, A., Quartararo, J., Tatè, R., Ghezzi, D., Zeviani, M., Goffrini, P., Ferrero, I., et al. (2013). The impairment of HCCS leads to MLS syndrome by activating a non-canonical cell death pathway in the brain and eyes. EMBO Mol. Med. *5*, 280–293. https://doi.org/10.1002/emmm.201201739.

Iorio, F., Isacchi, A., di Bernardo, D., Brunetti-Pierri, N., Mithbaokar, P., Ferriero, R., Murino, L., Tagliaferri, R., Brunetti-Pierri, N., Isacchi, A., and di Bernardo, D. (2010). Discovery of drug mode of action and drug repositioning from transcriptional responses. Autophagy *6*, 1204–1205. https://doi.org/10.1073/pnas.1000138107.

Jia, L., Srinivasula, S.M., Liu, F.T., Newland, A.C., Fernandes-Alnemri, T., Alnemri, E.S., and Kelsey, S.M. (2001). Apaf-1 protein deficiency confers resistance to cytochrome c-dependent apoptosis in human leukemic cells. Blood *98*, 414–421. https://doi.org/10.1182/blood.V98.2.414.

Katoh, I., Tomimori, Y., Ikawa, Y., and Kurata, S.i. (2004). Dimerization and processing of procaspase-9 by redox stress in mitochondria. J. Biol. Chem. *279*, 15515–15523. https://doi.org/10.1074/jbc.M311819200.

Khaliq, M., and Fallahi-Sichani, M. (2019). Epigenetic mechanisms of escape from BRAF oncogene dependency. Cancers *11*, 1480. https://doi.org/10.3390/cancers11101480.

Lampis, A., Carotenuto, P., Vlachogiannis, G., Cascione, L., Hedayat, S., Burke, R., Clarke, P., Bosma, E., Simbolo, M., Scarpa, A., et al. (2018). MIR21 drives resistance to heat shock protein 90 inhibition in cholangiocarcinoma. Gastroenterology *154*, 1066–1079.e5. https://doi.org/10.1053/j.gastro.2017.10.043.

Liu, J.R., Opipari, A.W., Tan, L., Jiang, Y., Zhang, Y., Tang, H., and Nuñez, G. (2002). Dysfunctional apoptosome activation in ovarian cancer: implications for chemoresistance. Cancer Res. *62*, 924–931.

Lopez-Bergami, P., Huang, C., Goydos, J.S., Yip, D., Bar-Eli, M., Herlyn, M., Smalley, K.S.M., Mahale, A., Eroshkin, A., Aaronson, S., and Ronai, Z. (2007). Rewired ERK-JNK signaling pathways in melanoma. Cancer Cell *11*, 447–460. https://doi.org/10.1016/j.ccr.2007.03.009.

Luke, J.J., Flaherty, K.T., Ribas, A., and Long, G.V. (2017). Targeted agents and immunotherapies: optimizing outcomes in melanoma. Nat. Rev. Clin. Oncol. *14*, 463–482. https://doi.org/10.1038/nrclinonc.2017.43.

Ma, X.-H., Piao, S.-F., Dey, S., Mcafee, Q., Karakousis, G., Villanueva, J., Hart, L.S., Levi, S., Hu, J., Zhang, G., et al. (2014). Targeting ER stress-induced autophagy overcomes BRAF inhibitor resistance in melanoma. J. Clin. Invest. *124*, 1406–1417. https://doi.org/10.1172/JCI70454.

Manns, J., Daubrawa, M., Driessen, S., Paasch, F., Hoffmann, N., Löffler, A., Lauber, K., Dieterle, A., Alers, S., Iftner, T., et al. (2011). Triggering of a novel intrinsic apoptosis pathway by the kinase inhibitor staurosporine: activation of caspase-9 in the absence of Apaf-1. Faseb. J. *25*, 3250–3261. https://doi.org/10.1096/fj.10-177527.

Mohapatra, P., Preet, R., Das, D., Satapathy, S.R., Choudhuri, T., Wyatt, M.D., and Kundu, C.N. (2012). Quinacrine-mediated autophagy and apoptosis in colon cancer cells is through a p53- and p21-dependent mechanism. Oncol. Res. *20*, 81–91. https://doi.org/10.3727/096504012X13473664562628.

Möller, K., Sigurbjornsdottir, S., Arnthorsson, A.O., Pogenberg, V., Dilshat, R., Fock, V., Brynjolfsdottir, S.H., Bindesboll, C., Bessadottir, M., Ogmundsdottir, H.M., et al. (2019a). MITF has a central role in regulating starvation-induced autophagy in melanoma. Sci. Rep. *9*, 1055. https://doi.org/10.1038/s41598-018-37522-6.

Morleo, M., Brillante, S., Formisano, U., Ferrante, L., Carbone, F., Iaconis, D., Palma, A., Buonomo, V., Maione, A.S., Grumati, P., et al. (2021). Regulation of autophagosome biogenesis by OFD1-mediated selective autophagy. EMBO J. *40*, e105120. https://doi.org/10.15252/embj.2020105120.

Nazarian, R., Shi, H., Wang, Q., Kong, X., Koya, R.C., Lee, H., Chen, Z., Lee, M.K., Attar, N., Sazegar, H., et al. (2010). Melanomas acquire resistance to B-RAF(V600E) inhibition by RTK or N-RAS upregulation. Nature *468*, 973–977. https://doi.org/10.1038/nature09626.

Paluncic, J., Kovacevic, Z., Jansson, P.J., Kalinowski, D., Merlot, A.M., Huang, M.L.H., Lok, H.C., Sahni, S., Lane, D.J.R., and Richardson, D.R. (2016). Roads to melanoma: key pathways and emerging players in melanoma progression and oncogenic signaling. Biochim. Biophys. Acta *1863*, 770–784. https://doi.org/10.1016/j.bbamcr.2016.01.025.

Pathria, G., Garg, B., Borgdorff, V., Garg, K., Wagner, C., Superti-Furga, G., and Wagner, S.N. (2016). Overcoming MITF-conferred drug resistance through dual AURKA/MAPK targeting in human melanoma cells. Cell Death Dis. *7*, e2135. https://doi.org/10.1038/cddis.2015.369.

Pecoraro, A., Carotenuto, P., Franco, B., De Cegli, R., Russo, G., and Russo, A. (2020). Role of uL3 in the crosstalk between nucleolar stress and autophagy in colon cancer cells. Int. J. Mol. Sci. *21*, E2143. https://doi.org/10.3390/ijms21062143.

Pellegrini, P., Serviss, J.T., Lundbäck, T., Bancaro, N., Mazurkiewicz, M., Kolosenko, I., Yu, D., Haraldsson, M., D'Arcy, P., Linder, S., and de Milito, A. (2018). A drug screening assay on cancer cells chronically adapted to acidosis. Cancer Cell Int. *18*, 147. https://doi.org/10.1186/s12935-018-0645-5.

Peltenburg, L.T.C., de Bruin, E.C., Meersma, D., Smit, N.P.M., Schrier, P.I., and Medema, J.P. (2005). Expression and function of the apoptosis effector Apaf-1 in melanoma. Cell Death Differ. *12*, 678–679. https://doi.org/10.1038/sj.cdd.4401630.

Perkins, C.L., Fang, G., Kim, C.N., and Bhalla, K.N. (2000). The role of Apaf-1, caspase-9, and Bid proteins in etoposide- or paclitaxel-induced mitochondrial events during apoptosis. Cancer Res. *60*, 1645–1653.

Rajkumar, S., and Watson, I.R. (2016). Molecular characterisation of cutaneous melanoma: creating a framework for targeted and immune therapies. Br. J. Cancer *115*, 145–155. https://doi.org/10.1038/bjc.2016.195.

Rao, R.v., Castro-Obregon, S., Frankowski, H., Schuler, M., Stoka, V., del Rio, G., Bredesen, D.E., and Ellerby, H.M. (2002). Coupling endoplasmic reticulum stress to the cell death program. J. Biol. Chem. *277*, 21836–21842. https://doi.org/10.1074/jbc.M202726200.

Smith, M.P., Brunton, H., Rowling, E.J., Ferguson, J., Arozarena, I., Miskolczi, Z., Lee, J.L., Girotti, M.R., Marais, R., Levesque, M.P., et al. (2016). Inhibiting drivers of non-mutational drug tolerance is a salvage strategy for targeted

melanoma therapy. Cancer Cell *29*, 270–284. https://doi.org/10.1016/j.ccell.2016.02.003.

Soengas, M.S., and Lowe, S.W. (2003). Apoptosis and melanoma chemoresistance. Oncogene *22*, 3138–3151. https://doi.org/10.1038/sj.onc.1206454.

Soengas, M.S., Capodieci, P., Polsky, D., Mora, J., Esteller, M., Opitz-Araya, X., McCombie, R., Herman, J.G., Gerald, W.L., Lazebnik, Y.A., et al. (2001). Inactivation of the apoptosis effector Apaf-1 in malignant melanoma. Nature *409*, 207–211. https://doi.org/10.1038/35051606.

Stoetzer, O.J., Pogrebniak, A., Pelka-Fleischer, R., Hasmann, M., Hiddemann, W., and Nuessler, V. (2002). Modulation of apoptosis by mitochondrial uncouplers: apoptosis-delaying features despite intrinsic cytotoxicity. Biochem. Pharmacol. *63*, 471–483. https://doi.org/10.1016/S0006-2952(01)00879-6.

Teijido, O., and Dejean, L. (2010). Upregulation of Bcl2 inhibits apoptosis-driven BAX insertion but favors BAX relocalization in mitochondria. FEBS Lett. *584*, 3305–3310. https://doi.org/10.1016/j.febslet.2010.07.002.

Tirosh, I., Izar, B., Prakadan, S.M., Wadsworth, M.H., Treacy, D., Trombetta, J.J., Rotem, A., Rodman, C., Lian, C., Murphy, G., et al. (2016). Dissecting the multicellular ecosystem of metastatic melanoma by single-cell RNA-seq. Science *352*, 189–196. https://doi.org/10.1126/science.aad0501.

Tomicic, M.T., Christmann, M., and Kaina, B. (2005). Apoptosis in UV-C light irradiated p53 wild-type, apaf-1 and p53 knockout mouse embryonic fibroblasts: interplay of receptor and mitochondrial pathway. Apoptosis *10*, 1295–1304. https://doi.org/10.1007/s10495-005-1392-3.

Umetani, N., Fujimoto, A., Takeuchi, H., Shinozaki, M., Bilchik, A.J., and Hoon, D.S.B. (2004). Allelic imbalance of APAF-1 locus at 12q23 is related to progression of colorectal carcinoma. Oncogene *23*, 8292–8300. https://doi.org/10.1038/sj.onc.1208022.

van Allen, E.M., Miao, D., Schilling, B., Shukla, S.A., Blank, C., Zimmer, L., Sucker, A., Hillen, U., Foppen, M.H.G., Goldinger, S.M., et al. (2015). Genomic correlates of response to CTLA-4 blockade in metastatic melanoma. Science *350*, 207–211. https://doi.org/10.1126/science.aad0095.

Wang, R., He, Y., Robinson, V., Yang, Z., Hessler, P., Lasko, L.M., Lu, X., Bhathena, A., Lai, A., Uziel, T., and Lam, L.T. (2018). Targeting lineage-specific MITF pathway in human melanoma cell lines by A-485, the selective small-molecule inhibitor of p300/CBP. Mol. Cancer Ther. *17*, 2543–2550. https://doi.org/10.1158/1535-7163.MCT-18-0511.

Wellbrock, C., and Arozarena, I. (2015). Microphthalmia-associated transcription factor in melanoma development and MAP -kinase pathway targeted therapy. Pigment Cell Melanoma Res. *28*, 390–406. https://doi.org/10.1111/pcmr.12370.

Wolf, B.B., Schuler, M., Li, W., Eggers-Sedlet, B., Lee, W., Tailor, P., Fitzgerald, P., Mills, G.B., and Green, D.R. (2001). Defective cytochrome c-dependent caspase activation in ovarian cancer cell lines due to diminished or absent apoptotic protease activating factor-1 activity. J. Biol. Chem. *276*, 34244–34251. https://doi.org/10.1074/jbc.M011778200.

Yamamoto, H., Gil, J., Schwartz, S., and Perucho, M. (2000). Frameshift mutations in Fas, Apaf-1, and Bcl-10 in gastro-intestinal cancer of the microsatellite mutator phenotype. Cell Death Differ. *7*, 238–239. https://doi.org/10.1038/sj.cdd.4400651.

Yokoyama, S., Feige, E., Poling, L.L., Levy, C., Widlund, H.R., Khaled, M., Kung, A.L., and Fisher, D.E. (2008). Pharmacologic suppression of MITF expression via HDAC inhibitors in the melanocyte lineage. Pigment Cell Melanoma Res. *21*, 457–463. https://doi.org/10.1111/j.1755-148X.2008.00480.x.

Yoshida, H., Kong, Y.Y., Yoshida, R., Elia, A.J., Hakem, A., Hakem, R., Penninger, J.M., and Mak, T.W. (1998). Apaf1 is required for mitochondrial pathways of apoptosis and brain development. Cell *94*, 739–750. https://doi.org/10.1016/S0092-8674(00)81733-X.

Zanon, M., Piris, A., Bersani, I., Vegetti, C., Molla, A., Scarito, A., and Anichini, A. (2004). Apoptosis protease activator protein-1 expression is dispensable for response of human melanoma cells to distinct proapoptotic agents. Cancer Res. *64*, 7386–7394. https://doi.org/10.1158/0008-5472.CAN-04-1640.

Zhang, J.H., Chung, T.D.Y., and Oldenburg, K.R. (1999). A simple statistical parameter for use in evaluation and validation of high throughput screening assays. J. Biomol. Screen *4*, 67–73. https://doi.org/10.1177/108705719900400206.

Zlobec, I., Minoo, P., Baker, K., Haegert, D., Khetani, K., Tornillo, L., Terracciano, L., Jass, J.R., and Lugli, A. (2007). Loss of APAF-1 expression is associated with tumour progression and adverse prognosis in colorectal cancer. Eur. J. Cancer *43*, 1101–1107. https://doi.org/10.1016/j.ejca.2007.01.029.

STAR★METHODS

KEY RESOURCES TABLE

REAGENT or RESOURCE	SOURCE	IDENTIFIER
Antibodies		
Rabbit monoclonal anti-APAF-1	Cell Signaling Technology	Cat#8969; RRID:AB_10859039
Rabbit monoclonal anti-PARP	Cell Signaling Technology	Cat# 9532; RRID:AB_659884
Rabbit monoclonal anti-cleaved PARP	Cell Signaling Technology	Cat# 5625; RRID:AB_10699459
Rabbit monoclonal anti-CASP-9	Cell Signaling Technology	Cat# 9505; RRID:AB_2290727
Rabbit monoclonal anti-cleaved CASP-3	Cell Signaling Technology	Cat# 9664; RRID:AB_2070042
Rabbit monoclonal anti-CASP-3	Cell Signaling Technology	Cat# 9662; RRID:AB_331439
Rabbit monoclonal anti-Phospho-p44/42 MAPK	Cell Signaling Technology	Cat# 4370; RRID:AB_2315112
Rabbit monoclonal anti- p44/42 MAPK	Cell Signaling Technology	Cat# 4695; RRID:AB_390779
Rabbit monoclonal anti-MITF	Cell Signaling Technology	Cat# 97800; RRID:AB_2800289
Rabbit monoclonal anti-Acetyl-Histone H3	Cell Signaling Technology	Cat# 8173; RRID:AB_10949503
Rabbit monoclonal anti-EZH2	Cell Signaling Technology	Cat# 5246; RRID:AB_10694683
Rabbit monoclonal anti-DNMT1	Cell Signaling Technology	Cat# 5032; RRID:AB_10548197
Rabbit monoclonal anti-tubulin	Cell Signaling Technology	Cat# 5335; RRID:AB_10544694
Rabbit polyclonal anti-LC3B	Novus	Cat# NB100-2220; RRID:AB_10003146
Mouse monoclonal anti-LAMP-1	Developmental Studies Hybridoma Bank	Cat# h4a3; RRID:AB_2296838
Mouse monoclonal anti-GAPDH	Proteintech	Cat# 60004-1-Ig; RRID:AB_2107436
Mouse monoclonal anti-Actin-b	Sigma-Aldrich	Cat# A5441; RRID:AB_476744
Rabbit monoclonal anti-Ki-67	Ventana Medical Systems	Cat# 790–4286; RRID:AB_2631262
Mouse monoclonal anti-MLANA	Ventana Medical Systems	Cat# 790–2990; RRID:AB_2336015
Mouse monoclonal anti-S100	Ventana Medical Systems	Cat# 790–2914
Mouse monoclonal anti-HMB45	Ventana Medical Systems	Cat# 790–4366, RRID:AB_2335979
Biological samples		
Melanoma Biopsies	Istituto Nazionale Tumori, IRCCS Fondazione “G. Pascale”, Naples, Italy	N/A
Chemicals, peptides, and recombinant proteins		
Prestwick Chemical Library®	Prestwick Chemical	Cat# 14D1305VP01ST02
FCCP (carbonyl cyanide p-trifluoromethoxyphenylhydrazone)	Sigma-Aldrich	Cat# C2920-10MG
Staurosporine	Sigma-Aldrich	Cat# S4400-5MG
Dabrafenib	Selleckchem	Cat# S2807-20MG
Trametinib	Selleckchem	Cat# S2673
Quinacrine	Prestwick Chemical	Cat# PRESTW-318-1
Methylbenzethonium chloride	Prestwick Chemical	Cat# PREST-705-1
Chloroquine	Sigma-Aldrich	Cat# C6628
Rapamycin	Millipore	Cat# 553210-1MG
Lipofectamine™ 2000 Transfection Reagent	Invitrogen Life Technologies	Cat# 11668019
DMEM 1X	ThermoFisher Scientific	Cat# 41965–039
Sirtinol	Selleckchem	Cat# S2804
Trichostatin A	Promega	Cat# G6560
HBSS 1X_	ThermoFisher Scientific	Cat# 14025–092
CASPASE 9 INHIBITOR Z-LEHD-FMK	CALBIOCHEM	Cat# 218761
CASPASE 3–7 INHIBITOR Z-VAD-FMK	CALBIOCHEM	Cat# 627610
Hoechst 33342 Solution	ThermoFisher Scientific	Cat# 62249

(*Continued on next page*)

Continued

REAGENT or RESOURCE	SOURCE	IDENTIFIER
CellEvent™ Caspase-3/7 Green Detection Reagent	ThermoFisher Scientific	Cat# C10423
Crystal violet	Bio Basic Inc.	Cat#: CB0331
Critical commercial assays		
Caspase-Glo9_assay	Promega	Cat#: G8211
Caspase-Glo 3/7 assay	Promega	Cat#: G8091
Annexin V: FITC Apoptosis Detection Kit I	BD	Cat#: BD556547
Maxwell RSC RNA FFPE Kit	Promega	Cat#: AS1440
CellTiter 96(R) AQueous One Solution Kit	Promega	Cat#: G3580
Maxwell® RSC simplyRNA Cells Kit	Promega	Cat#: AS1390
QuantiTect® Reverse Transcription Kit	Qiagen	Cat#: 205311
LightCycler® 480 SYBR Green I Master Mix Kit	Roche Life Science	Cat#: 4887352001
Click-iT TUNEL Colorimetric IHC Detection Kit	ThermoFisher Scientific	Cat#: C10625
HDAC-Glo™ I/II Screening System	Promega	Cat#: G6420-30
TruSeq RNA Library Prep Kit v2	Illumina	Cat#: RS-122-2001/2
TruSeq PE Cluster Kit v3-cBot-HS	Illumina	Cat#: PE-401-3001
Fluorogenic HDAC Assay Kits	BPS Bioscience	Cat# 50022–53001
Deposited data		
Raw and analyzed RNA-seq data	This paper	GEO: GSE214541; GEO: GSE214473
Experimental models: Cell lines		
A375	ATCC	CRL-1619
M14	ATCC	HTB-129
SK-MEL-28	ATCC	HTB-72
PES-43	Istituto Nazionale Tumori IRCCS Fondazione “G. Pascale”	N/A
M230	Istituto Nazionale Tumori IRCCS Fondazione “G. Pascale”	N/A
LOX-IMIV	Istituto Nazionale Tumori IRCCS Fondazione “G. Pascale”	RRID:CVCL_1381
SK-MEL-2	ATCC	HTB-68
MALME-3M	ATCC	HTB-64
MEL-501	Istituto Nazionale Tumori IRCCS Fondazione “G. Pascale”	N/A
UACC-257	Istituto Nazionale Tumori IRCCS Fondazione “G. Pascale”	RRID:CVCL_1779
M257	Istituto Nazionale Tumori IRCCS Fondazione “G. Pascale”	RRID:CVCL_D757
Mouse Embryonic Fibroblast APAF-1 KO	TIGEM core facility	N/A
Melanoma biopsies derived primary cells MMC49B	Isolated in study	N/A
Melanoma biopsies derived primary cells MMC35	Isolated in study	N/A
Melanoma biopsies derived primary cells MMC49	Isolated in study	N/A
Melanoma biopsies derived primary cells MMC936	Isolated in study	N/A
Melanoma biopsies derived primary cells LCP-Mel	Isolated in study	N/A
Melanoma biopsies derived primary cells WM-266-Mel	Isolated in study	N/A
Melanoma biopsies derived primary cells LCM-Mel	Isolated in study	N/A
A375-APAF1KO melanoma cells	Obtained in this study	N/A
Experimental models: Organisms/strains		
Mouse: BALB/c	Charles River	RRID:IMSR_CRL:028

(*Continued on next page*)

Continued

REAGENT or RESOURCE	SOURCE	IDENTIFIER
Oligonucleotides		
gRNA sequence for CRISPR-CAS9 gene editing of CASP9: GCTACTCGCCATGGACGAAG	This Paper	N/A
PCR Primers for genotyping CASP9-KO clones: CASPup GTGGGGAGCGAAGACTGAC, CASP9low CTGCCTCCTCTGGTCATTCC	This Paper	N/A
Primers for RT-PCR analyses can be found in Table S8	This paper	N/A
Recombinant DNA		
pCRISPR-CG12 Cas9 nuclease expression clone	GeneCopoeia	CP-C9NU-01
mRFP-eGFP-LC3B	Morleo et al. (2021)	N/A
pcs2-Bcl-2	Indrieri et al. (2013)	N/A
Software and algorithms		
Columbus Image Data Storage and Analysis System	PerkinElmer	https://www.perkinelmer.com/
Prism v8.0	Graphpad	https://www.graphpad.com
ImageJ	NIH	https://imagej.nih.gov/ij/
MANTRA	Iorio et al. (2010)	https://mantra.tigem.it/
Swiss Target Prediction	Iorio et al. (2010); Daina et al. (2019)	http://www.swisstargetprediction.ch/
Zeiss Zen 2012 software	Zeiss	https://www.zeiss.it/microscopia/local-content/zen-software-tutori.html
RSEM version 1.2.25	Barbato et al. (2021)	http://deweylab.biostat.wisc.edu/rsem
Other		
Bioanalyzer	Agilent Technologies	https://www.agilent.com/en/product/automated-electrophoresis/bioanalyzer-systems/bioanalyzer-instrument
Qubit 2.0 Fluorometer	ThermoFisher Scientific	https://www.thermofisher.com/it/en/home/references/newsletters-and-journals/bioprobes-journal-of-cell-biology-applications/bioprobes-issues-2011/bioprobes-64-april-2011/the-qubit-2-0-fluorometer-april-2011.html
Novaseq6000 platform	Illumina	https://www.illumina.com/systems/sequencing-platforms/novaseq.html
BD Accuri C6 Analyzer	BD	https://www.bdbiosciences.com/en-us/products/instruments/flow-cytometers/research-cell-analyzers/bd-accuri-c6-plus
LightCycler 96	Roche	https://lifescience.roche.com/en_it/products/lightcycler-381711.html
Glomax Discovery System	Promega	https://ita.promega.com/products/microplate-readers-fluorometers-luminometers/microplate-readers/glomax-discover-system/?catNum=GM3000
Operetta HTS imaging System	PerkinElmer	https://www.perkinelmer.com/uk/category/operetta-cls-high-content-analysis-system

RESOURCE AVAILABILITY

Lead contact

Further information and requests for resources and reagents should be directed to and will be fulfilled by the lead contact, Pietro Carotenuto (p.carotenuto@tigem.it).

Materials availability

All unique/stable reagents generated in this study are available from the lead contact with a completed Materials Transfer Agreement.

Data and code availability

- All RNAseq data have been deposited at at the Gene Expression Omnibus (GEO) database and are publicly available as of the date of publication. Accession number is listed in the key resources table.
- This paper does not report original code.
- Any additional information required to reanalyze the data reported in this paper is available from the lead contact upon request.

EXPERIMENTAL MODEL AND SUBJECT DETAILS

Patient samples

Patients with mutant $BRAF^{V600}$-positive metastatic melanoma were treated with either a BRAF inhibitor, or a combination of BRAF and MEK inhibitors (for patient characteristics see Table S1). All patients consented for tissue acquisition as per an institutional-review-board-approved protocol (Office for Human Research Studies, Dana-Farber/Harvard Cancer Center). Tumor biopsies were obtained at time of progression if applicable. The study was conducted according to the guidelines of the Declaration of Helsinki and approved by the Ethics Committee of Istituto Nazionale Tumori-IRCCS-Fondazione "G. Pascale", Naples, Italy (date of registration 18/01/2018; project identification code n° 33/17 oss, 2018). Total RNA from FFPE tissues was isolated using Maxwell RSC RNA FFPE kit (Promega, Madison, WI, USA) and processed with Maxwell RSC Instrument (Promega, Madison, WI, USA) as described in (Barbato et al., 2021).

Cell lines and patient-derived cells

Cell lines (A375, M14, SK-MEL-28, PES-43, M230, LOX IM IV, SK-MEL-2, MALME-3M, MEL-501, UACC-257, M257, Mouse embryonic fibroblast (MEF) APAF-1 KO) were obtained from the American Type Culture Collection (ATCC, Manassas, VA, USA) or from partner institutes (MMC49B, MMC35, MMC49, MMC936, LCP-Mel, WM-266-Mel, LCM-Mel). Due to the genetic deletion of APAF-1, MEF APAF-1 KO are unable to initiate apoptosome-dependent mitochondrial apoptosis and show significant resistance to a variety of apoptotic stimuli, including UV irradiation and genotoxic reagents (Andreu-Fernández et al., 2013; Cecconi et al., 1998; Perkins et al., 2000; Tomicic et al., 2005; Yoshida et al., 1998).

Authentication of cell lines was done by Eurofins GmbH and confirmed by online STR-matching analysis (www.dsmz.de/fp/cgi-bin/str.html). All cells were grown in RPMI 1640 (Invitrogen, Karlsruhe, Germany) with L-Glutamine, 10% fetal bovine serum (FCS), 100U/mL penicillin, and 50μg of streptomycin.

Establishment of the primary cells (described in Table S4) from metastatic melanomas was previously described in Elgendy et al. (2014, 2019). Briefly, tumor biopsies obtained from patients were shred in Petri dishes containing RPMI 1640 + 10% FCS with a scalpel. Cell suspension was filtered through sterile gauze to eliminate macroscopic debris and then incubated with DNase (200UI ml^{-1}), collagenase (0.1%), hyaluronidase (2.5UI ml^{-1}) and Trypsin (0.5mg mL^{-1}) for 45-min at room temperature on a magnetic shaker. Cells in suspension were filtered through sterile gauze to remove debris, recovered by centrifugation and extensively washed in RPMI 1640 + 10% FCS. Cells were grown in DMEM +10% FBS and were characterized by immunohistochemistry staining with S100, MLANA and HMB45 (1:1000, Ventana Medical Systems, USA) antibodies at various passages in culture. Mycoplasma testing of the cell lines was performed every three months.

Tissue biopsies of metastatic melanomas were collected from patients whose informed consent was obtained in writing according to the policies of the Ethics Committee of the European Institute of Oncology and regulations of the Italian Ministry of Health. NRAS and BRAF gene variant analysis was performed by standard sequencing at Cogentech (Milan, IT). Characteristics of LCP-Mel, WM-266-Mel and LCM-Mel patient-derived cell lines are described in (Gentilcore et al., 2013).

MAPKi-resistant cells were generated by continuous selective culture as following described. Dabrafenib-resistant melanoma cells (A375-BIR) were selected by growing the 2 melanoma cell lines in medium containing increased concentrations of dabrafenib for 4 weeks. A375 and M14 melanoma cell lines resistant to 1μM dabrafenib were selected. MEK inhibitor resistant cell lines (A375-DR) were obtained by partner institutions (PAA, MC, GP).

METHOD DETAILS

Transfection

The pcs2 or pcs2-Bcl-2 plasmids were directly transfected into the cells using Lipofectamine™ 2000 Transfection Reagent (Invitrogen Life Technologies, Carlsbad, CA, USA) according to the manufacturers protocol. SiRNA reagents and controls were purchased from Dharmacon Horizon Discovery, Cambridge, UK). Transfection with 40nM nM siRNA and/or negative control mimics was performed with Lipofectamine™ 2000 reagent (Invitrogen Life Technologies, Carlsbad, CA, USA).

Generation of CASP9 gene knockout in A375 cells

CASP9 gene knockout (KO) in A375 cells was generated by using the CRISPR/Cas9 system. CRISPR/Cas9 system was purchased from GeneCopoeia (Rockville, MD). To drive the expression of the Cas9 protein, Cas9 nuclease expression clone was specifically designed to have CMV promoter, a mammalian antibiotic resistance gene as a stable selection marker (Neo), and a reporter gene, mCherry fluorescent protein. The selected gRNA which sequence is: GCTACTCGCCATGGACGAAG, targets the ATG of the *CASP9* gene (NM_001229.5). FACS-sorted single-cell clones were genotyped by PCR reaction with the specific primers: CASPup GTGGGGAGCGAAGACTGAC, CASP9low CTGCCTCCTCTGGTCATTCC. PCR products were analyzed by DNA Sanger sequencing and the cell clone carrying the INDEL mutations c.1 *DEL* **ATG**GACGAAGCGGATCGGCGG was selected and expanded.

High-throughput compound screening

The Prestwick Chemical Library® was used for the High-throughput compound screening (HTS) in this study. The library was purchased from Prestwick Chemicals (Washington, DC) and comprises 1280 molecules, supplied as 10 mM stock solutions in DMSO.

Cells were plated at 3000 cells/well in flat-bottom 384-wells plate (Greiner Bio-One, Monroe, NC; 781091) for fluorometric assays, left under the laminar hood for 1h and then moved to the incubator. On the next day, the library was diluted 1:100 with DMEM containing 10% FBS and added to the plated cells. All plates were treated simultaneously with 10μM of each of the compounds from the Prestwick chemical library (one compound per well). For each plate, twelve wells were used as negative controls (DMSO at final percentage of 0.01%) and twelve wells used for the positive control (FCCP 20μM). FCCP (carbonyl cyanide p-trifluoromethoxyphenylhydrazone) has been selected as main positive control, since it is able to activate the apoptosome-independent cell death pathway (Indrieri et al., 2013). FCCP is a well-documented mitochondrial membrane pore opener implicated in the induction of mitochondria-based apoptotic cell death (Stoetzer et al., 2002). The concentration of FCCP (20 μM) has been selected on the basis of a dose-response apoptotic assay, and it corresponds to the effective dose able to induce apoptosis in 60% of MEF APAF-1 KO cells (Figure S2C).

Library addition was performed using the Hamilton Microlab STAR Liquid Handling System (Hamilton Company, Reno, NV, USA). Plates were assayed 8h after compound addition using immunofluorescent staining and high-content imaging approaches as detailed below. Compound precipitation was visually assessed on addition and on imaging (Lampis et al., 2018).

After treatment, cells were stained with Hoechst 33342 (ThermoFisher Scientific) and CellEvent Caspase-3/7 Green Detection Reagent (ThermoFisher Scientific) for 30min before fixation. After some PBS washes, plates were scanned and images collected with an Operetta HTS imaging system (Perkin Elmer, Waltham, MA) at 20× magnification with 12 fields of view (510 × 675 μm)/well. Images were then analysed with Columbus 2.2 (Perkin Elmer, Waltham, MA).

We used CellEvent® Caspase-3/7 Green (Thermo Fisher Scientific) for the detection of activated CASP-3/7. CellEvent® Caspase-3/7 Green reagent is a four amino acid peptide (DEVD) conjugated to a nucleic acid-binding dye that is nonfluorescent when not bound to DNA because the DEVD peptide inhibits binding of the dye to DNA. When cleaved caspase-3/7 is expressed in apoptotic cells, the DEVD peptide is cleaved, and the free dye can bind DNA, generating a green fluorescence.

The Operetta High-content/high-throughput imaging system and Columbus algorithms were devised to identify changes in nuclear morphology and apoptosis as main endpoints, by using Hoechst and CellEvent® fluorescent staining, respectively. The first component of the algorithm was designed to assess alterations in cell number and nuclear morphology. A second algorithm component was added to identify apoptotic cells, defined as nucleated cells stained with the green CASP-3/7 reagent. These parameters were then combined in a single image algorithm that identified the percent of apoptotic-positive cells.

The resulting cell-level measurements of Hoechst 33342 (ThermoFisher Scientific) and activated CASP-3/7 fluorescent intensity were exported and analyzed utilizing customized scripts in R. The screening window coefficient (Z'-factor) was used as an indicator for assay development and optimization (i.e., setting of cell number, exposure time, volumes used, etc.) and as a statistical tool for the assay quality assessment (Zhang et al., 1999). The quality of the assay was considered sufficient for screening and automation when Z'-factor >0.5. Z'-factor was determined using FCCP as a positive control and DMSO as a negative control. The Z'-factor was calculated according to the formula: Z' = 1–3(SdPos + SdNeg)/AvPos−AvNeg, where SD and Av are the standard deviation and the average, respectively, of the percentage of apoptotic cells of the negative (AvNeg) and positive control wells (Zhang et al., 1999). Compounds with a Normalized Percent of Apoptosis (NPI) score superior to 30% (apoptosis induction superior to 30%) and with a Robust Z-Score (Z-Score) greater than 4 were considered positive hits in primary screening. NPI and Z-Score were calculated across plates for the main phenotypic endpoints, based on the negative controls (0.1% DMSO) for the screening batch (12 plates, 36 negative and positive controls/batch and 144 negative and positive controls overall/batch). Z-Score and NPI were calculated using the following formulas: Z-score = (Av Sample Value-MedianValues)/MADValues; NPI = (Avpos – AvSample)/(Avneg - AvSample) x

100%, where MedianValue and MADValue are respectively the median and the median absolute deviation (MAD) of all sample values. In NPI calculation, Av values are the average of percentage of apoptotic cells of the negative control (AvNeg), positive control (AvPos), and Sample (AvSample) wells (Buchser et al., 2014).

Selected hits were then arrayed in 384-well plates and tested in a double validation screening using the same experimental procedures described above for the primary screening. Compounds with NPI >40% and Z-Score > 5 were selected as positive hits.

For the HTS screening in melanoma cells, the two hit compounds (QNC and MBZ) together with FCCP (20μM; Sigma-Aldrich), Staurosporine (20μM) (Sigma-Aldrich) and DMSO control were arrayed in 384-well white plates, at target concentrations of 30, 10, 3.33, 1.11, 0.37, 0.12μM. Eight hours after co-incubation with melanoma cells, the % of apoptotic cells has evaluated as described before.

Dabrafenib (DABR) and trametinib (TRAM) were purchased from Selleckchem (Munrgeseich, Germany); QNC (Quinacrine) and MBZ (Methylbenzethonium chloride) from Prestwick Chemicals (Washington, DC).

Caspase activity assay

Following treatments cells were subjected to CASP-3/7, 9 activities measurement with Caspase-Glo assay kit (Promega, Madison USA). Briefly, the plates containing cells were removed from the incubator and allowed to equilibrate to room temperature for 30min. 50μL of Caspase-Glo reagent was added to each well, the content of well was gently mixed with a plate shaker at 300–500 rpm for 30sec. The plate was then incubated at room temperature for 2h (Carotenuto et al., 2021). The luminescence of each sample was measured in a plate-reading luminometer (GloMax Discover System, Promega) with parameters of 1 min lag time and 0.5 s/well-read time. The experiments were performed in triplicate and repeated on two separately initiated cultures. CASP-9 (Z-LEHD-FMK) and -3–7 (Z-VAD-FMK) specific inhibitors were used following manufacturer instructions (Calbiochem).

For the HTS validation screening, hit compounds were arrayed in 384-well white plates as described before, at target concentrations of 30, 10, 3.33, 1.11, 0.37, 0.12μM. Eight hours after co-incubation with cells, Caspase 3/7, 9 activities were evaluated.

Western blot analysis

The cells were lysed with RIPA buffer containing protease and phosphatase inhibitors (Selleckchem). The protein concentration was tested with a BCA kit, and appropriate amounts of protein were prepared for SDS-PAGE and then transferred to PVDF membrane (Millipore, MA, USA). The membranes were blocked for 1h with 5% non-fat dry milk and then incubated with rabbit anti-APAF-1 mAb (1:1000; #8969; Cell Signaling Technology Europe, Netherlands); rabbit anti-PARP mAb (1:1000; #9532; Cell Signaling Technology Europe, Netherlands); rabbit anti-cleaved PARP mAb (1:1000; #5625; Cell Signaling Technology Europe, Netherlands); rabbit anti-CASP9 mAb (1:1000; #9505; Cell Signaling Technology Europe, Netherlands); rabbit anti- Cleaved Caspase-3 mAb (1:1000; #9664; Cell Signaling Technology Europe, Netherlands); rabbit anti-Caspase-3 mAb (1:1000; #9662; Cell Signaling Technology Europe, Netherlands); rabbit anti-Phospho-p44/42 MAPK (p-Erk1/2; 1:1000; #4370; Cell Signaling Technology Europe, Netherlands); rabbit anti-p44/42 MAPK (Erk1/2; 1:1000; #4695; Cell Signaling Technology Europe, Netherlands); rabbit anti-MITF (1:1000; #97800; Cell Signaling Technology Europe, Netherlands); rabbit anti-Acetyl-Histone H3 (1:1000; #8173; Cell Signaling Technology Europe, Netherlands); rabbit anti-EZH2 (1:1000; #5246; Cell Signaling Technology Europe, Netherlands); rabbit anti-DNMT1 (1:1000; #5032; Cell Signaling Technology Europe, Netherlands); Rabbit polyclonal anti-LC3B (1:1000; #NB100-2220; Novus Biologicals-Bio-Techne Ltd, UK). Additionally, anti-b-tubulin (1:1000; #5335; Cell Signaling Technology Europe, Netherlands), GAPDH (1:3000; 60004-1-Ig; Proteintech, Manchester, UK), Actin-b (1:5000, A5441; Sigma; St. Louis, MO, USA) mABs were used as loading controls. The results were imaged using a gel image analysis system (Bio-Rad, California, USA) according to the manufacturer's instructions.

Quantitative real-time PCR analysis

Total RNA was extracted from the cell samples using Trizol reagent (Invitrogen, California, USA) or in alternative Maxwell RSC simplyRNA Cells (Promega) and processed with Maxwell RSC Instrument (Promega) according to the manufacturer's instructions. Reverse transcription reaction was performed using the Quantitect Reverse Transcription kit (Qiagen) following the manufacturer's directions. Quantitative RT-PCR was performed in LightCycler 96 (Roche, Penzberg, Germany) using LightCycler FastStart DNA Master SYBR Green I (Roche) and each validated primer. Validated qRT-PCR primers were from Eurofins (Milan). GAPDH was used as an internal control. The primer sequences are listed in Table S8.

Proliferation assay

For proliferation assay (CellTiter 96® Non-Radioactive Cell Proliferation Assay-MTT, Promega), 1.0×10^5 cells were plated onto 96-well plates for overnight incubation and subjected to the experimental treatments indicated. At the designated time-points, 20μL of freshly prepared MTT solution was added to individual wells (containing 200μL cell culture media) and incubated at 37°C for 3h. Absorbance measurements were recorded using GloMax Discover System (Promega) multi-well microplate reader (absorbance 492 nm). GI_{50} was defined as the dose required to decrease cell viability by 50% after 48h. GI_{50} analysis for patient derived melanoma cells was performed cells by treating cells with a series of concentrations of QNC, MBZ, DABR, TRAM alone, or DABR and TRAM in combination with 1 or 2 μM of QNC and MBZ for 48h.

The GI_{50} was determined from the regression of a plot of the logarithm of the concentration versus percent inhibition by Graph Pad Prism (version 8) using the Dose-Response One-Site Model.

Colony formation assay

The cells were seeded onto 24-well plates (200cells/well) and treated with indicated compounds or DMSO (Vehicle) for 7–10 days. Resistance or sensitivity to DABR was assessed by treating cell lines with DABR alone (200nM) or in combination with QNC or MBZ (1–2 μM) and DMSO. After washing and fixation, the cells were stained with 0.5% Crystal Violet (Bio Basic Inc., Markham, Canada) in 25% methanol for 10min. Cell colonies were then photographed and counted.

Annexin V-FITC/PI staining assay

Cells were treated with indicated compounds and DMSO control for 48h, and the cell apoptosis was measured by using Annexin V-FITC/PI Apoptosis Detection Kit (BD Biosciences, San Diego, CA, USA). Cells were suspended in binding buffer, stained with Annexin V-FITC and PI for 15 min at room temperature in dark. Apoptotic cells were analyzed using a BD Accuri C6 Analyzer (BD Biosciences, San Diego, CA, USA).

Animal studies

Female BALB/c nude mice (5 weeks old) were purchased from the Charles River Laboratories. Eighteen mice were divided randomly into 3 groups, including the vehicle group (saline solution), the 30mg/kg QNC group and the 5 mg/kg MBZ group. A375 and M14 cells (2×10^6) were subcutaneously injected into the flanks of mice. When the tumors reached 200mm^3, each group of mice was injected through intraperitoneal injection with the corresponding drugs twice per week for 6 weeks. The tumor size was measured using a caliper three times a week, and the tumor volume was calculated with the formula V = 1/2 (length × $width^2$). When the tumors reached 1000 mm^3, the mice were sacrificed, and the tumors were collected. The tumors were photographed. Furthermore, the tumor sections were immunostained (Carotenuto et al., 2020).

HDAC assays

HDAC-Glo reagents were purchased from Promega, Madison, WI. Fluorogenic assay kits for specific isoforms were acquired from BPS Bioscience (San Diego, CA). The fluorogenic assays were performed for individual HDAC enzymes (BPS Bioscience) using human recombinant enzymes and fluorogenic HDAC substrates. Briefly, a 50μL buffer (50mM Tris-HCl, pH7.4, 137mM NaCl, 2.7mM KCl, 0.05% Tween-20, and 5μg/mL BSA) mixture containing the human recombinant HDAC enzyme isoform test compound and the corresponding HDAC substrate was added into a black 96-well assay plate. The reaction in each well was incubated at 37°C for 30min, followed by adding 50μL of HDAC Developer reagent and incubated at room temperature for an additional 20min. Fluorescence intensity of the assay plates was measured on an microplate reader. The fluorescence intensity data was analyzed using Prism (GraphPad Software, La Jolla, CA). The DSMO controls (Ft) and enzyme-free controls (Fb) were defined as 100% and 0% HDAC activity respectively. The percent activity of each compound was calculated as (F-Fb)/(Ft-Fb), where F represents the fluorescence intensity value at the specified compound concentration. TCA, SIRT (20μM), QNC, MBZ (2μM) were tested with individual recombinant HDAC class enzymes and their corresponding fluorogenic substrates. Trichostatin A (Promega) and Sirtinol (Sellechem) were used as specific HDACs inhibitors.

Immunohistochemistry analysis

Tissue sections were deparaffinized and subjected to antigen retrieval. The endogenous peroxidase was blocked using 3% hydrogen peroxide. The slides were first blocked with normal goat serum at room temperature for 30 min to minimize nonspecific staining, then incubated overnight with primary antibodies against Caspase-3, CASP-3 (1:1000, Cell Signaling Technology Europe, Netherlands), Caspase-9, CASP-9 (1:1000, Cell Signaling Technology Europe, Netherlands), Ki67 (1:1000, Ventana Medical Systems, USA), MLANA (1:1000, Ventana Medical Systems, USA). Subsequently, the slides were incubated with HRP-labelled goat anti-rabbit/mouse secondary antibody at 37°C for 20min, counter-stained with hematoxylin, dehydrated, and stabilized with mounting medium. The detection of apoptotic cells was done by the Click-iT™ TUNEL Colorimetric IHC Detection Kit (Thermofisher Scientific).

RNAseq library preparation and deep sequencing

For RNA-seq analysis, libraries were prepared using TruSeq RNA Sample Preparation kit, (Illumina) starting from 4μg of total RNA as described in (Pecoraro et al., 2020). Quality control of library templates was performed using a High Sensitivity DNA Assay kit (Agilent Technologies) on a Bioanalyzer (Agilent Technologies). The Qubit quantification platform (Qubit 2.0 Fluorometer, ThermoFisher Scientific) was used to normalize samples for the library preparation. Using multiplexing, up to 6 samples were combined into a single lane to yield sufficient coverage. The sequencing was carried out in collaboration with the Next Generation Sequencing (NGS) Facility at TIGEM. Cluster generation was performed on Flow Cell v3 (TruSeq PE Cluster Kit v3; Illumina) using cBOT. Libraries were sequenced by a paired-end chemistry on an NovaSeq6000 platform. Each library was loaded at a concentration of 8pM, which was previously established as optimal. An average yield of ~4.5 Mb was obtained per sample (Barbato et al., 2021). The data have been deposited in NCBIs Gene Expression Omnibus (GEO; see key resources table) (Edgar et al., 2002).

Bioinformatic analysis

A data analysis was performed using the pipeline already established at the Bioinformatics and Statistics Core Facility at TIGEM (Pecoraro et al., 2020; Barbato et al., 2021). Briefly, the reads were trimmed to remove adapter sequences and low-quality ends and reads mapping to contaminating sequences (e.g., ribosomal RNA, phIX control) were filtered-out. Reads were aligned and assigned to Human ENSEMBLE transcripts and genes (hg38 reference) by using RSEM version 1.2.25 with standard parameters (Pecoraro et al., 2020; Barbato et al., 2021). The threshold for statistical significance chosen was False Discovery Rate (FDR) < 0.05. The Gene set enrichment analysis (GSEA) was then performed restricting the output to the collection of ''hallmark'' and ''Biocarta'' gene sets part of the Molecular Signatures Database (MSigDB v7.0) (Pecoraro et al., 2020; Barbato et al., 2021). The threshold for statistical significance chosen in the GSEA was False Discovery Rate (FDR) < 0,25. The expression of differentially induced/suppressed genes (FDR < 0.05) was validated by RT-PCR.

Computational target prediction

The computational prediction of target was performed by using following: MANTRA (Iorio et al., 2010) and Swiss Target Prediction (Daina et al., 2019) as reported by (Iorio et al., 2010; Daina et al., 2019). Data obtained from both tools were compared, scored and used to identify epigenetic target classes. Data are available upon request from the lead contact.

cBioPortal analysis

RNA sequencing data (in format V2 RSEM Z-score) of SKCM-DFCI cohort of metastatic melanoma (van Allen et al., 2015) were retrieved from the cBioPortal for Cancer Genomics interface (http://www.cbioportal.org/) used to generate gene lists composed of expression correlated genes for MITF and APAF-1. Correlation coefficients were calculated before the Log2 transformation of RNA sequencing data. Log2 transformed RNA sequencing data were used for heat map, hierarchical clustering, and survival analysis.

Immunofluorescent staining and imaging

Cells were seeded on slides and fixed for 10min with Methanol (Sigma-Aldrich), followed by incubation with blocking–permeabilization solution: 0.5% BSA, 0.1% saponin, and NH_4Cl 50mmol/L in phosphate buffered saline for 30 min. Primary antibodies anti-LC3B (Novus Biologicals-Bio-Techne Ltd, UK) and anti-LAMP1 (H4A, Developmental Studies Hybridoma Bank, Iowa City, IA, USA) were diluted in blocking–permeabilization solution and added to the cells for 1h. Then, secondary antibodies were incubated for 45min. Lastly, cells were counterstained with Hoechst (Thermo Fisher Scientific, USA). Samples were examined under a confocal microscope (Zeiss LSM 700; Carl Zeiss AG, Jena, Germany) equipped with 40× and 63 × 1.4 NA oil objective. Co-localization between specific markers was quantified using Zeiss Zen 2012 software (Zeiss LSM 700; Carl Zeiss AG, Jena, Germany).

Quantification of autophagy inhibition

Cells were plated at 50,000 cells per well in RPMI with 10% FBS on 1.5 coverglass in 24-well tissue culture plates and transiently transfected with a plasmid encoding an mRFP–GFP-tagged LC3 (mRFP-eGFP-LC3B) provided by A. Fraldi (TIGEM, Pozzuoli, Italy) (Morleo et al., 2021). After transfection, cells were kept in growth medium for 3h and then incubation was continued in normal growth medium or the cells were treated with HBSS for 3h. Then, cells were treated with rapamycin (100nM) (Millipore, 553210–10mg), CQ (25μM), Dabrafenib (200nM), FCCP (20μM), QNC (2μM) and MBZ (2μM) for 4h. Chloroquine (CQ) (Ma et al., 2014) is a lysosomal degradation inhibitor used as control. Cells were washed with 1× PBS, fixed with 3.7% formaldehyde, and nuclei were stained with Hoechst-33342 (2μg/mL). Coverglass was inverted onto microscope slides using mounting gel. Samples were examined under a confocal microscope (Zeiss LSM 700; Carl Zeiss AG, Jena, Germany) equipped with 40× and 63 × 1.4 NA oil objective. Co-localization between specific markers was quantified using Zeiss Zen 2012 software. Puncta number was used to measure autophagy inhibition, which is the statistically significant ($p \leq 0.05$) increase in mRFP-eGFP-LC3B-labeled puncta number compared with DMSO control, determined by the Student t test as described in (Morleo et al., 2021). Mean intensity was further chosen for quantification as it accurately represents both the increase in puncta number and area when the accumulation of autophagosomes partially fuse. Quantification of the red channel (RFP-LC3 puncta) was performed to determine the total autophagic vesicle population (both autophagosomes and autolysosomes). Autofluorescence of each compound was tested using wild-type cells to confirm that compound autofluorescence did not interfere with quantification. Regions of interest (ROI) were drawn around the edges of each cell. Intensity thresholds were set to include all pixels equal to or greater than the intensity of the mean background fluorescence using the separation feature and restrictions set for puncta size. Objects within the threshold for each ROI were quantified using an automated object count function and exported for analysis. Although other parameters were also collected, the mean intensity of the objects was averaged between the 10 images of each concentration, or approximately 50 cells. The effects of QNC and MBZ on autophagy was also examined using LC3 conversion (determined by immunoblotting analysis) as an indicator of autophagosomal accumulation and autophagic degradation (Figures S6M–S6P).

QUANTIFICATION AND STATISTICAL ANALYSIS

Statistical analysis

The sample sizes for each experiment are indicated in the figures (different dots in graphs) as well as in figure legends. Statistical tests including Student's *t* test, Wilcoxon's rank-sum test and One-way ANOVA with Bonferroni's or Tukey's multiple comparison test were performed with Prism GraphPad (GraphPad Software 8.0, La Jolla California, USA). Data are presented as mean +/- SD. Results were considered statistically significant if $p < 0.05$.

The calculation of the GI_{50} values were performed with GraphPad Prism (GraphPad Software 8.0, La Jolla California, USA) and followed a nonlinear regression model applied to the sigmoidal dose-response curves of the cell viability data. The values were log-transformed before fitting the model.

To decrease data overfitting, the criteria used for significant expression correlation between two genes was a Pearson correlation coefficient $r \geq 0.3$ or ≤ -0.3, a Spearman correlation coefficient $r \geq 0.4$ or ≤ -0.4, and all corresponding p values < 0.05.

For survival data, Kaplan–Meier curves were plotted and compared using a log-rank test. All tests were two-sided.